Postseismic gravity changes observed from GRACE satellites:
The two components of postseismic gravity changes and the mechanisms of them

重力衛星 GRACE を用いた地震後重力変化の研究:
余効変動の二成分の分離とそのメカニズムの考察

Space Geodesy, Earth and Planetary Dynamics
Department of Natural History Sciences,
Graduate School of Science, Hokkaido University

Yusaku Tanaka

Supervisor: Prof. Kosuke Heki

北海道大学 大学院 理学院 自然史科学専攻
地球惑星ダイナミクス講座 宇宙測地学研究室

田中優作

指導教官:日置幸介 教授

February 2014

ABSTRACT

The time series analysis of the gravity changes of the three M_w9-class mega-thrust earthquakes, i.e. the 2004 Sumatra-Andaman earthquake, the 2010 Chile (Maule) earthquake, and the 2011 Tohoku-oki earthquake, provides the possibility to identify their multiple postseismic phenomena. We have three sensors for earthquakes. The first sensor is seismometers, and we can measure seismic waves with them. The second sensor, such as GNSS (Global Navigation Satellite System) and SAR (Synthetic Aperture Rader), can measure crustal movements associated with earthquakes. The third sensor is gravimetry. The first sensor cannot catch the signal of postseismic phenomena because they do not shake the ground. The second sensor can catch the signal of postseismic phenomena, but they cannot separate phenomena, such as afterslip and viscous relaxation, because these mechanisms let the ground move in the same polarity. However, these postseismic processes may result in different polarities in gravity changes. This suggests that the gravity can be a powerful sensor to separated signals of different postseismic processes.

GRACE (Gravity Recovery And Climate Experiment) is the twin satellite systems launched in 2002 by NASA (National Aeronautics and Space Administration) and DLR (German Space Agency). It provides the two-dimensional gravity field of the earth with high temporal and spatial resolution. GRACE gives us insights into mass movements beneath the surface associated with earthquakes. The gravity time series before and after large earthquakes with GRACE suggest that the gravity (1) decreases coseismically, (2) keeps on decreasing for a few months, and (3) increases over a longer period. In other words, the postseismic gravity changes seem to have two components, i.e. the short-term and the long-term components. This new discovery suggests that the gravity observations detected two different postseismic processes with opposite polarities.

The mechanisms of coseismic gravity changes are relatively well known but those of short- and long-term postseismic gravity changes are not so clear at the moment. They are explained with afterslip and viscoelastic relaxation to some extent, but problems still remain. Nevertheless, the gravity observation can do what seismometers and GNSS/SAR cannot do, i.e. to separate different postseismic processes giving rise to gravity changes in different polarities.

概要

本研究では，重力衛星 GRACE (Gravity Recovery And Climate Experiment) が捉えた超巨大逆断層型地震（2004 年スマトラーアンダマン地震，2010 年チリ（マウレ）地震，2011 年東北沖地震）に伴う重力変化を時系列解析することで，重力が地震後に地球内部で起こっている現象を分離して観測できる第一の手段になりうることを示した．地震を観測するセンサーは今のところ三種類ある．第一のセンサーは地震計であり，第二のセンサーは GPS (Global Positioning System) を始めとする GNSS (Global Navigation Satellite System)及び SAR (Synthetic Aperture Rader)などの宇宙技術を用いた地殻変動の観測手法，そして重力観測が第三のセンサーである．地震計は地震波を捉え，GNSS や SAR は地殻変動を空から観測し，重力は質量移動を追跡する．地震「時」の現象はどのセンサーでも捉えることができる．しかし地震「後」の現象は，地震波を出さないため地震計では捉えられない．地震後の地表の動きは GNSS や SAR が捉えることができる．しかし，それらも地下で複数のメカニズム（余効すべりや粘弾性緩和）による過程が起こっていた場合，それらを分離して捉えることは難しい．可能なのは，いくつかの仮定を置いた上で，複数の現象に対応したモデル計算を行い，その結果と観測結果の一致を得ることである．しかし，地震後に複数のメカニズムで変動が起こっている場合，もっと望ましいのは，そのメカニズムの各々を別々に観測値として得ることだろう．本研究で発見したのは，地震後に起こる変動が重力としては、逆の極性でかつ異なる時間スケールで観測されることである．これは重力が地震後に地球内部で起こっている現象を区別して観測できる第一の手段である可能性を強く示している．

CONTENTS

1 Introduction

1.1 Space Geodesy in geoscience

Space geodesy is the discipline of the shape, size, gravity fields, rotation, and so on, of the earth, other planets, and the moon with space techniques. Geodesy with satellite started in 1957, when the first satellite "Sputnik I" was launched by the Soviet Union. Space geodesy has been applied to many disciplines in geoscience, and has contributed to their advances. For example, GPS (Global Positioning System) and SAR (Synthetic Aperture Radar) are applied to seismology, volcanology, meteorology, solar terrestrial physics, and so on. This is because observations from satellites are often superior to those on the ground in various aspects. One is the temporal continuity: satellites keep providing observation data until they stop functioning. Another aspect is that huge amount of data will eventually become available to researchers, giving all scientists chances to study using such data. One more aspect is that satellites often give two-dimensional observation data with uniform quality. This cannot be achieved by deploying many sensors on the ground. These aspects make space geodesy a very important approach in geosciences.

1.2 Satellite gravimetry

Gravity measurements in general have played and will continue to play important roles in earth sciences because they provide much information on the matters beneath the surface that we cannot see directly; the gravity fields reflect how mass is distributed there.

Satellite gravimetry started in 1958, when USA launched the satellite "Vanguard I". Tracking of this satellite enabled us to estimate low degree/order gravity field of the earth for the first time. Satellite gravimetry can be done in several different ways. The first one is SLR (Satellite Laser Ranging), which started in late 1960s. Satellites for SLR have a lot of corner-cube-reflectors (CCR) on their surfaces. The CCRs reflect laser pulses emitted from the ground station, and people can measure the two-way travel times of the laser pulses between the ground station and the satellites. The changes in orbital elements depend on the gravity, so we can recover the gravity field model. SLR has some benefits. First of all, it is relatively easy to continue the operation of SLR satellites because they have only passive function to reflect laser pulses with CCRs (they do not need batteries). Another benefit is that SLR is a relatively old technique, and we can go back further in time.

The second type is composed of "twin" satellites, and is represented by GRACE (Gravity Recovery And Climate Experiment), launched in 2002. The gravity irregularities change not only the orbital parameters of satellites but also their velocities. Then, the relative velocity between the two satellites tells us how different the gravity fields are between the two satellites.

GRACE has good spatial and temporal resolution. The spatial resolution of GRACE is 300~500 km. This is much better than that of SLR because the GRACE orbit is much lower than SLR satellites. For example, LAGEOS, one of the most useful SLR satellites, has an orbit as high as about 6000 km. The temporal resolution of GRACE is about one month, which is better than GOCE (Gravity field and steady-state Ocean Circulation Explorer), the third type of satellites to measure the gravity field with an on-board gradiometer. GOCE is called "Ferrari of the satellites" because it flies the lowest orbit of the satellites (this means its speed is the highest). GOCE has the best spatial resolution of the three types. Each type of satellites has its benefit and has produced valuable sets of data.

1.3 Gravity and earthquakes

Gravity observation is considered to be the third approach to understand earthquakes. The first sensor is seismometers to observe elastic (seismic) waves, and the second sensor is GNSS (Global Navigation Satellite System) like GPS and SAR to observe static displacement of the ground surface. Gravimetry, the third sensor, can observe the mass transportation under the ground.

There are two kinds of gravity changes due to earthquakes: co- and postseismic gravity changes (we do not discuss preseismic changes here). The mechanisms responsible for coseismic gravity changes have been understood to a certain extent. The coseismic gravity change occurs in two processes, i.e. (1) vertical movements of the boundaries with density contrast, such as the surface and Moho, and (2) density changes in mantle and crust. They are further separated into four: surface uplift/subsidence, Moho uplift/subsidence, dilatation and compression within crust and mantle. For submarine earthquakes, movement of sea water also plays a secondary role. These mechanisms are shown in Figure 1.1. The mechanisms of postseismic gravity changes are, however, not so clear.

Coseismic gravity change was first detected after the 2003 Tokachi-oki earthquake (M_w8.0), Japan, by a ground array of superconducting gravimeters [*Imanishi et al.*, 2004]. The second example (also the 1^{st} example with satellite gravimetry) was coseismic gravity changes by the 2004 Sumatra-Andaman earthquake (M_w9.2) detected by the GRACE satellites [*Han et al.*, 2006]. Satellite gravimetry enabled similar studies for the 2010 Maule (M_w8.8) [*Heki and Matsuo*, 2010; *Han et al.*, 2010] and the 2011 Tohoku-Oki (M_w9.0) [*Matsuo and Heki*, 2011; *Wang et al.*, 2012] earthquakes. These reports showed that coseismic gravity changes are dominated by the decrease on the back arc side of the ruptured fault reflecting the density drop of rocks there [*Han et al.*, 2006].

Postseismic gravity changes were first found for the 2004 Sumatra-Andaman earthquake [*Ogawa and Heki*, 2007; *Chen et al.*, 2007]. They showed that the gravity increased after coseismic decreasing (Figure1.2) by fitting the function (1.1) with the least-squares method. They also revealed that postseismic gravity changes show opposite polarity and slight trenchward shift, i.e. gravity increase occurred directly above the ruptured fault.

For the other two M_w9-class earthquakes (2010 Maule and 2011 Tohoku), the time series of postseismic gravity changes have not been reported yet. Here we use the newly released Level-2 (RL05) GRACE data, which were improved in accuracy [*Dahle et al.*, 2012; *Chambers and Bonin*, 2012], and study common features in the co- and postseismic gravity changes of these megathrust earthquakes.

I model the gravity G as a function of time t as follows,

$$G = a + bt + c\,sin(\omega t + \theta_1) + d\,sin(2\omega t + \theta_2) + H(t)\left\{\Delta g + e\left(1 - \exp\left(\frac{\Delta t}{\tau}\right)\right)\right\} \quad (1.1)$$

$$H(t) = \begin{cases} 0 \ (t < t_0) \\ 1 \ (t \geq t_0) \end{cases}$$

$$\Delta t = t - t_0$$

where *a, b, c, d,* and *e* are the constants to be estimated with the least-squares method, t_0 is the time when the earthquake occurred, the second term means the secular trend, the third and fourth terms correspond to the seasonal changes ($\omega \equiv 2\pi/1\text{yr}$), Δg is the coseismic gravity step, and the last term is the postseismic gravity change. $H(t)$ is the step function, and τ is the time constant.

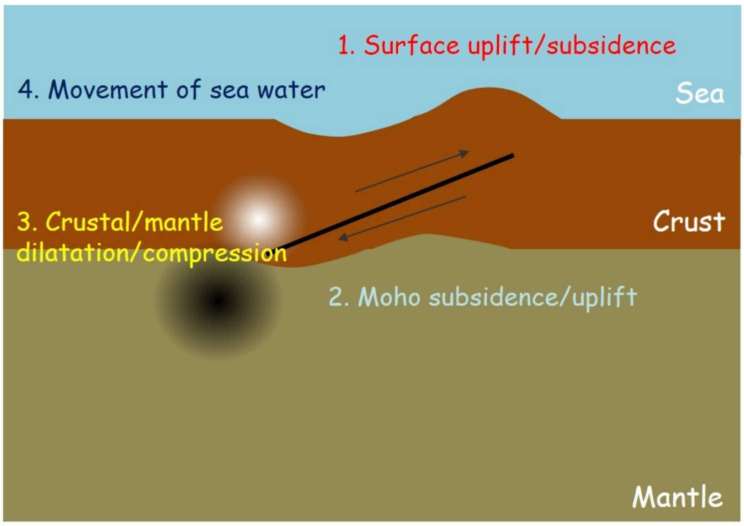

Figure 1.1 The four major mechanisms responsible for coseismic gravity changes.

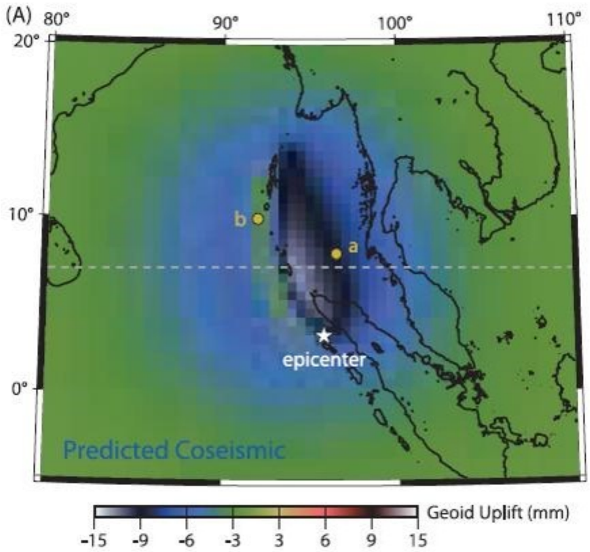

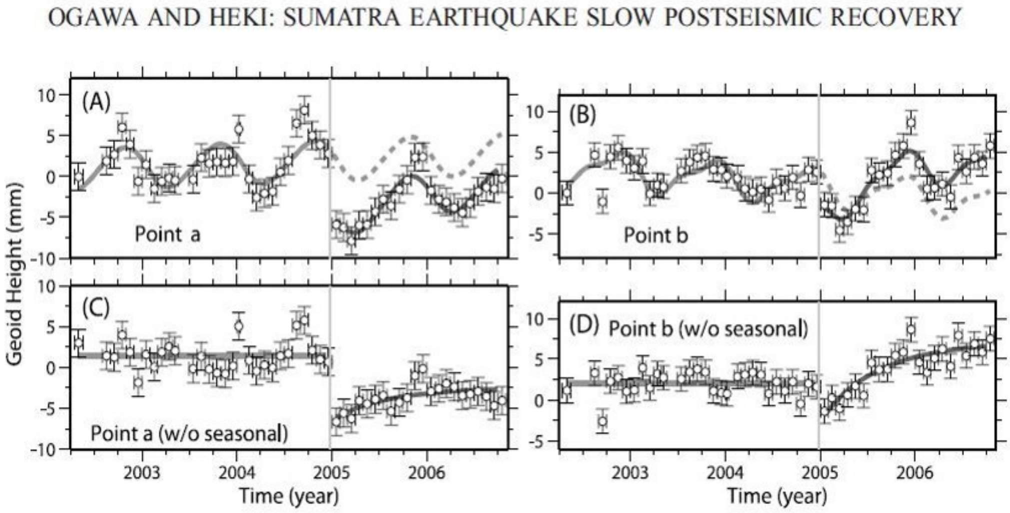

Figure 1.2 The postseismic geoid height changes of the 2004 Sumatra-Andaman earthquake shown by *Ogawa and Heki* [2007]. The geoid height decreased when the earthquake occurred and increased slowly afterwards.

2 Data and Methods

2.1 GRACE data

GRACE data can be downloaded from http://podaac.jpl.nasa.gov/ (PO.DAAC: Physical Oceanography Distributed Active Archive Center) or http://isdc.gfz-potsdam.de/ (ISDC:

Information Systems and Data Center). These data are provided by the three research centers, i.e. UTCSR (University of Texas, Center for Space Research), JPL (Jet Propulsion Laboratory), and GFZ (GeoForschungsZentrum, Potsdam). UTCSR and JPL are in USA, and GFZ is in Germany. These three institutions analyze data based on somewhat different approaches so the data sets differ slightly from center to center.

There are three levels of GRACE data available to the users: Level-1B, Level-2, and Level-3. Level-1B gives the data of the ranges (distances) between the twin satellites together with their changing rates, and it takes some expertise in technical details to use them. Level-2 data are provided as spherical harmonic coefficients, and we need only certain mathematical knowledge to use them. Level-3 data are composed of space domain gravity data after being filtered in several ways. Because it takes neither technical nor mathematical knowledge to use them, Level-3 is the most friendly to users. However, Level-3 data do not give us much information because many filters have already been applied. In this study, Level-2 data analyzed at UTCSR are used.

Level-2 data are composed of spherical harmonic coefficients (Stokes' coefficients). They coefficients can be converted to the static gravity field $g(\theta, \phi)$ of the earth by the equation (2.1) [*Kaula*, 1966; *Heiskanen and Moritz*, 1967].

$$g(\theta,\varphi) = \frac{GM}{R^2}\sum_{n=2}^{nmax}(n-1)\sum_{m=0}^{n}(C_{nm}\cos m\varphi + S_{nm}\sin m\varphi)\overline{P_{nm}}(\sin\theta) \qquad (2.1)$$

Where G is the universal gravity constant, M is the mass of the earth, R is the equatorial radius, $P_{nm}(\sin\theta)$ is the n-th degree and m-th order fully-normalized associated Legendre function. An example of the static gravity field of the earth is shown in the figure 2.1.

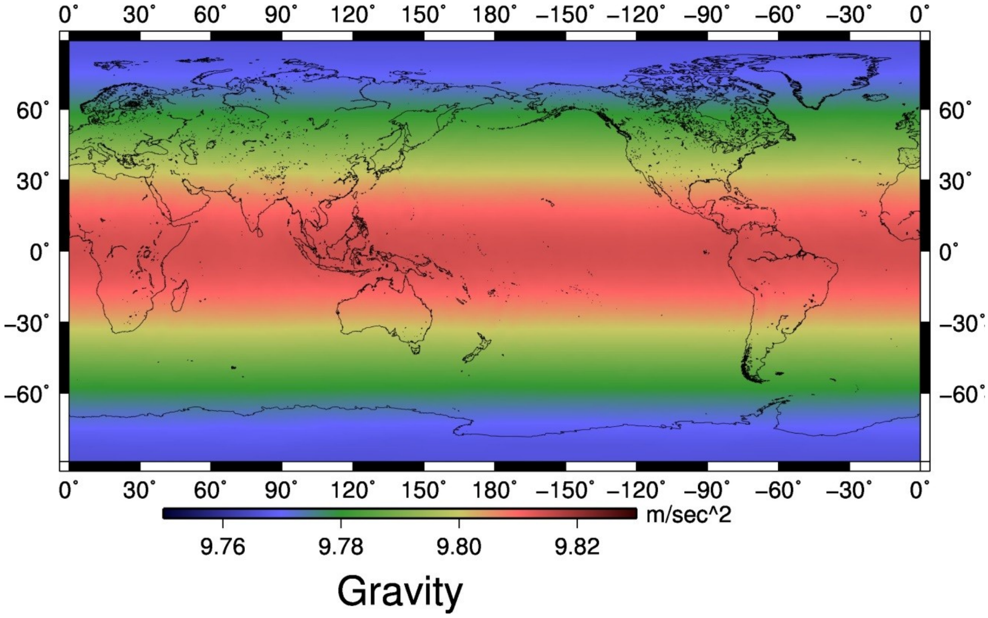

Figure 2.1 The map of the static gravity field of the earth in November 2013 calculated from Level-2 GRACE data. Degrees and orders of spherical harmonic coefficients are up to 60.

Figure 2.1 shows the mean of the gravity is about 9.8 m/s^2 and the gravity on lower latitude is stronger than that on higher. But this is contradictory to the fact that the gravity on lower latitude is weaker because the centrifugal force of the rotation of the earth works. The reason of this contradiction is that the gravity fields measured by satellites do not include centrifugal forces and gravitational pull of the equatorial bulge is isolated. Because the C_{20} term predominates in the earth's gravity fields, I removed it and plot the rest of the gravity components in figure 2.2. When we discuss time-variable gravity, we use C_{20} from SLR observations because C_{20} values by GRACE are less accurate.

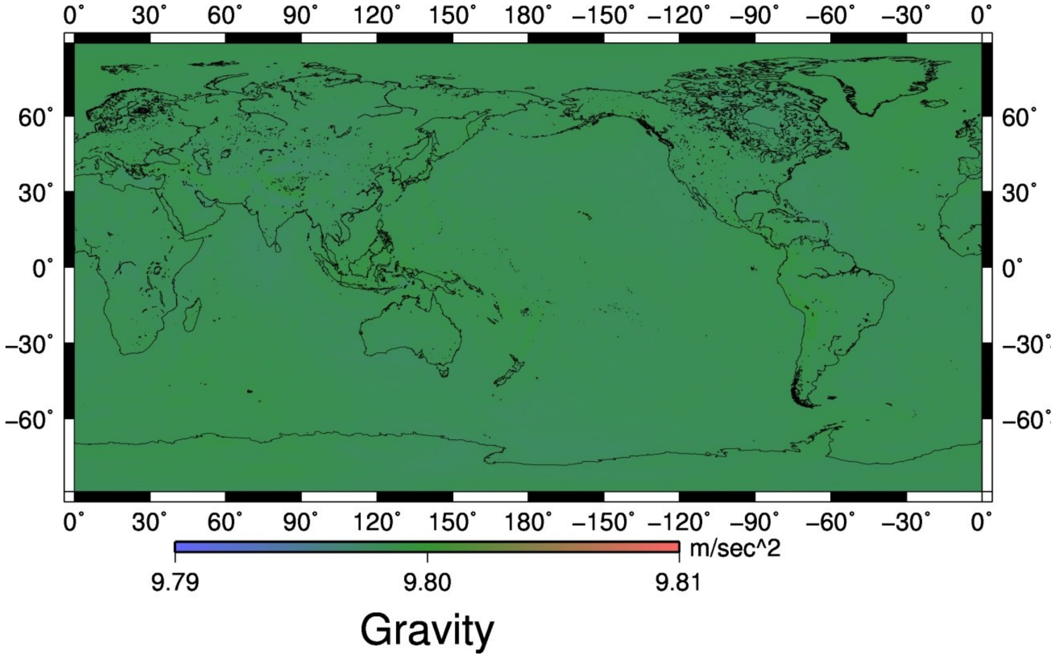

Figure 2.2 The map of the static gravity field of the earth in November 2013 calculated from Level-2 GRACE data after removing the C_{20} component.

Figure 2.2 shows that the gravity anomaly is so small that gravity is uniformly 9.8 m/s^2 throughout the surface. In order to highlight the gravity anomalies, we should use the unit of mGal (1Gal = 1cm/s^2) and should also make C_{00} zero because it gives the mean value of the gravity field. Figure 2.3 and figure 2.4 show the gravity anomaly with the unit mGal.

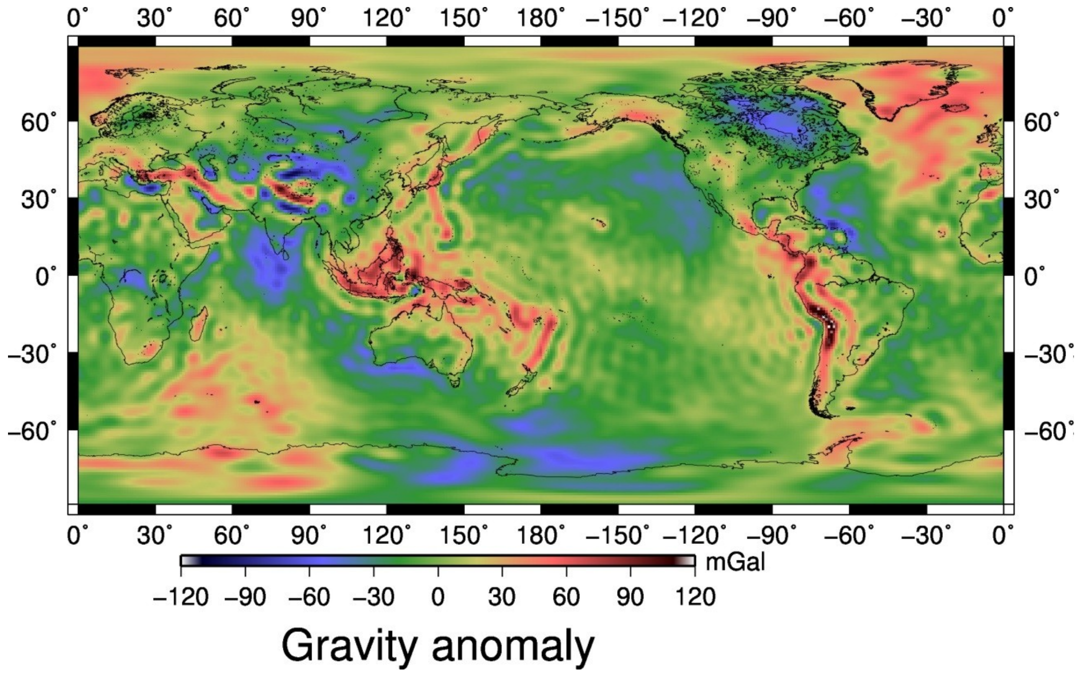

Figure 2.3 The map of the static gravity anomaly of the earth in November 2013 calculated from Level-2 GRACE data. I removed the C_{20} and C_{00} components.

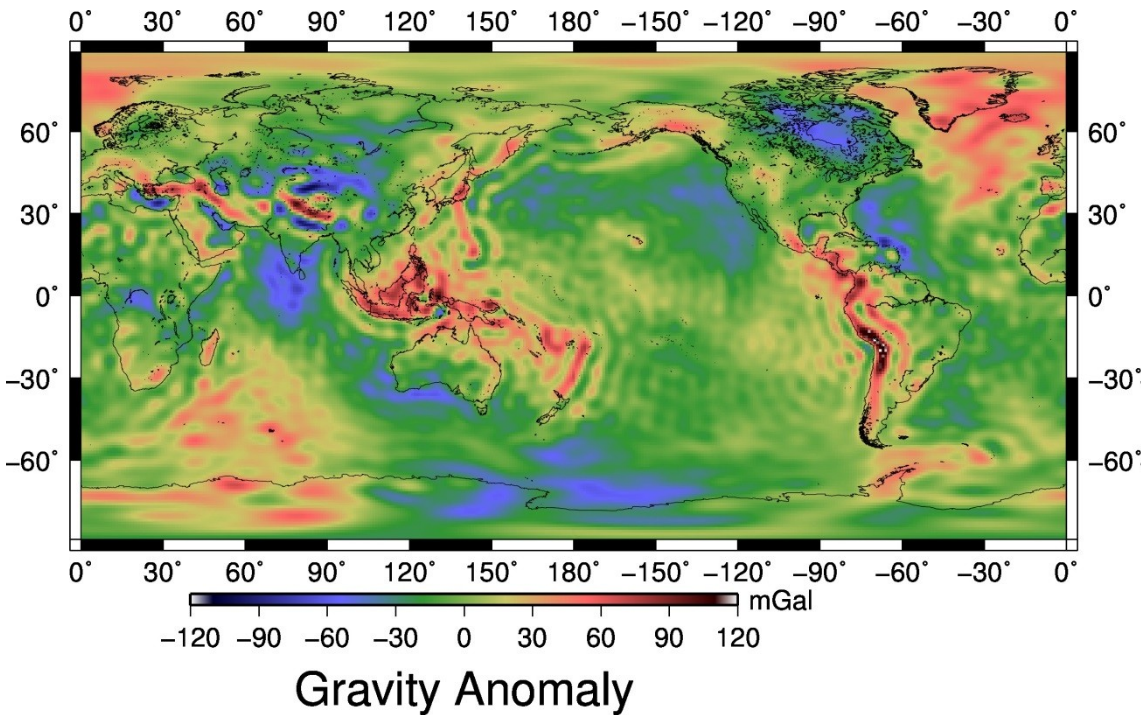

Figure 2.4 The map of the static gravity anomaly of the earth in October 2013 calculated from Level-2 GRACE data. I removed the C_{20} and C_{00} components. This looks almost identical to figure 2.3.

Figures 2.3 and 2.4 show the gravity anomaly in November and October, respectively. They represent different time epochs, but they look alike because the temporal changes of the gravity fields are small. In order to study time-variable gravity, we have to use the unit of μGal. Figure 2.5 shows the difference of the gravity fields in November 2013 from October 2013.

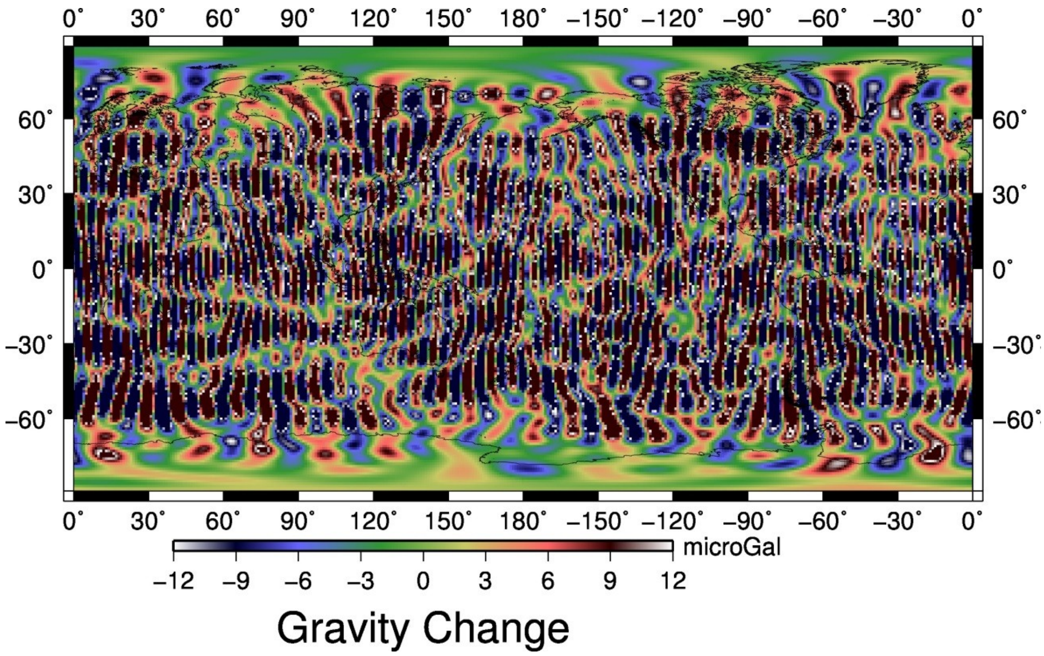

Figure 2.5 The gravity fields in November relative to those in October 2013.

Figure 2.5 shows the strong north-south stripes. These stripes appear because GRACE data are noisy in short-wavelength components; GRACE satellites orbit the earth in a polar circular orbit at the altitude of about 500 km, taking about 90 minutes per one cycle (they experience about 550 revolutions every month). This suggests that we have to take certain means to analyze (e.g. applying special filters) time variable gravity with the GRACE data.

One way to avoid these stripes is to use northward components rather than the downward component of the gravity field. The north components do not show the stripes because the GRACE satellites move in the north-south direction. We can calculate this by differentiating the gravity potential with respect to the latitude. Figure 2.6 shows the distribution of the northward component of the gravity changes between October and November, 2013.

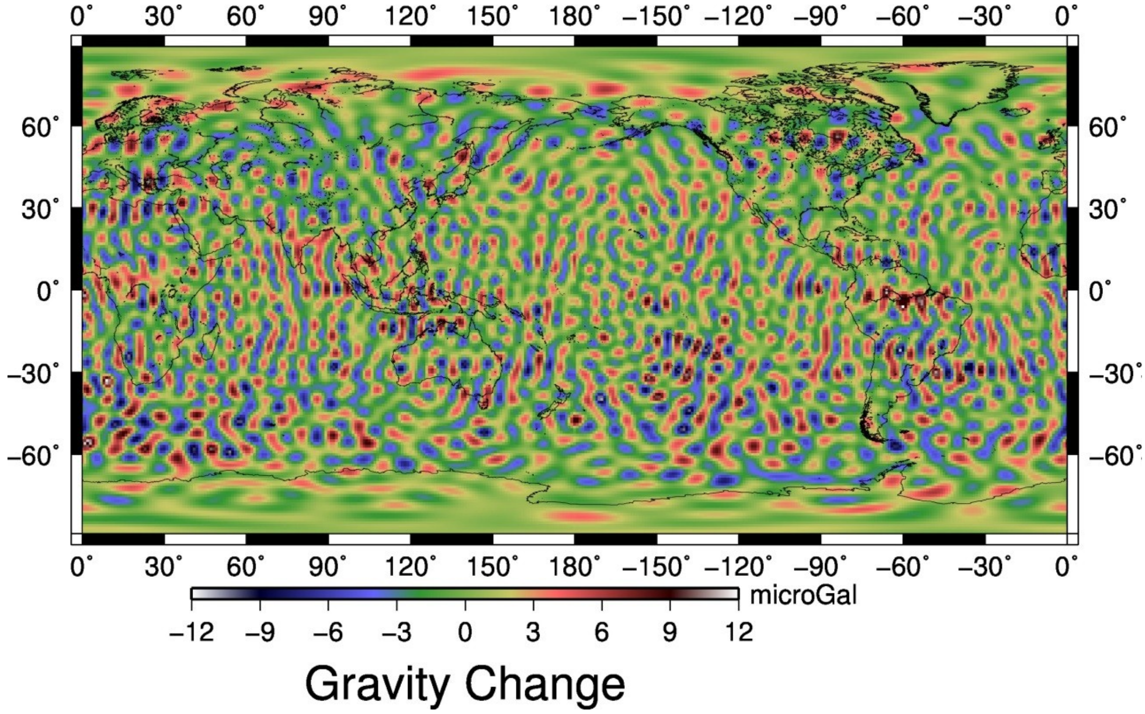

Figure 2.6 The northward component of the gravity changes from October to November in 2013. Strong north-south stripes in figure 2.5 have disappeared.

The northward gravity changes observed with GRACE satellites are shown in figure 2.6. They are largely free from strong stripes although short wavelength noises still remain. After all, we have to apply additional filters to GRACE data.

2.2 Spatial filters

2.2.1 De-striping filter

The filter to remove stripes is called de-striping filter proposed by *Swenson and Wahr* [2006]. They found that the stripes come from the highly systematic behavior of the Stokes' coefficients in the GRACE data. The Stokes' coefficients of C_{n16} are shown in figure 2.7 as an example. There the red points (the evens of coefficients) are always bigger than blue points (odds) when n is larger than 30 and black line connecting them goes zigzag strongly. *Swenson and Wahr* [2006] considered that this is responsible for the stripes, and tried to suppress the stripes by getting rid of this systematic behavior. To do that, two polynomial functions were fitted with the least-squares method to each evens and odds of coefficients separately, and residuals between the values of original data and the fitted polynomial were taken as the new "de-striped" coefficients. Figure 2.8 shows the gravity change calculated with the de-striped coefficients. This de-striping filter is called as P5M10, which means that polynomials of degree 5 were fitted to the coefficients of degrees and orders 10 or more.

In this section, the gravity changes were calculated at first and then the de-striping filter was given because this order makes sense to understand the de-striping filter. Practically, the de-striping filter is applied to the data at first, and then the gravity changes are calculated to obtain the time series.

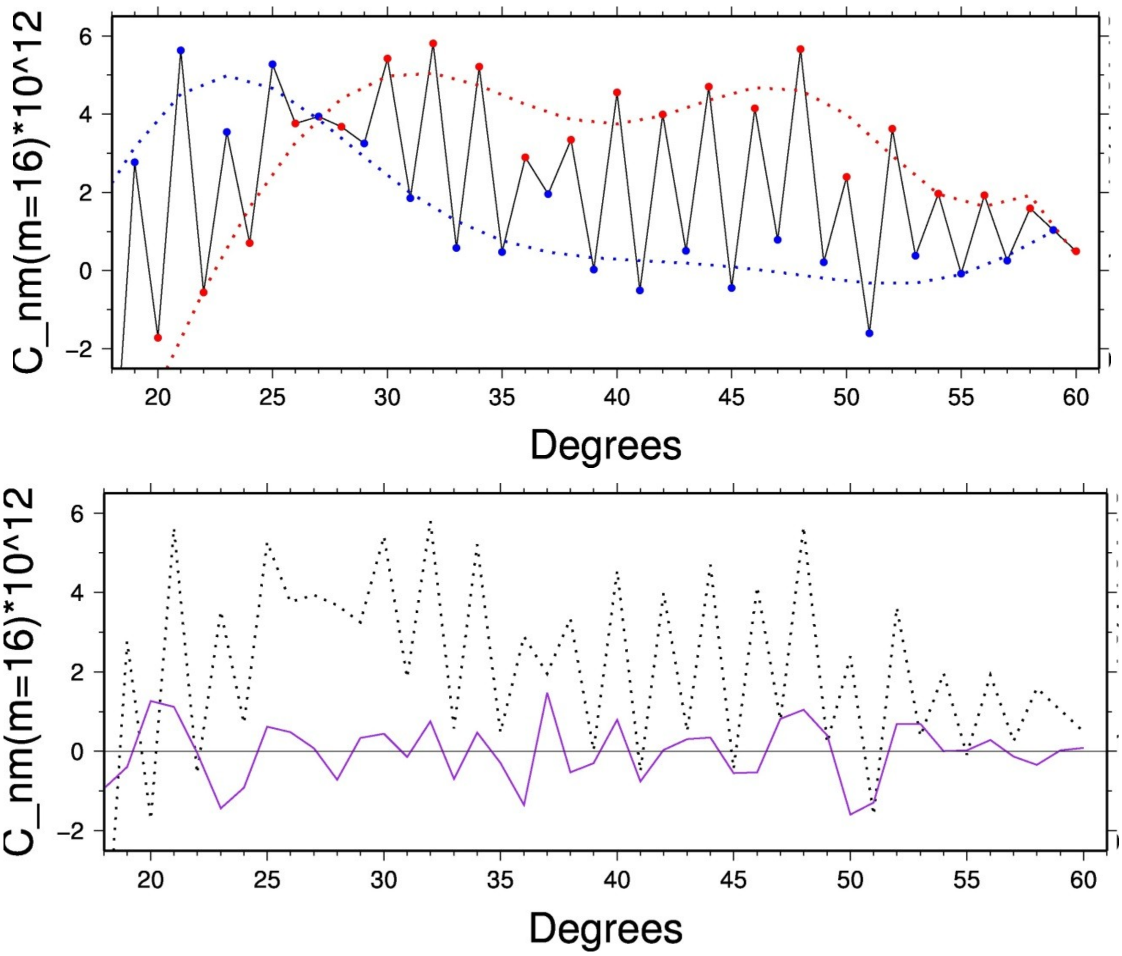

Figure 2.7 This figure gives conceptual explanation of the de-striping filter. (above) The solid black line indicate the Stokes' coefficients of order 16, i.e. ΔC_{n16} (C_{n16} in November 2013 – C_{n16} in October 2013) as a function of degree n. The red points denote the values of coefficients with even n and blue points denote those with odd n. The broken lines are the curves fitted to each color's data with polynomial degrees = 10. (below) The broken black line is the same line of the solid black line above. The purple line shows the difference between the black line and the fitted polynomial curves. The horizontal straight line means zero.

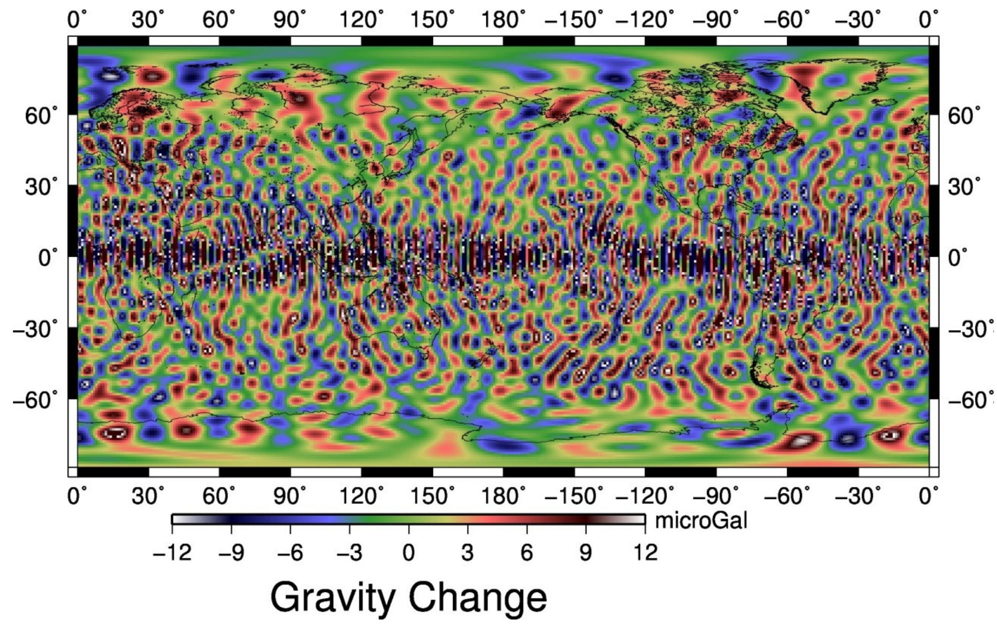

Figure 2.8 The gravity change in from October to November 2013 calculated with the "de-striped" coefficients.

Figure 2.8 shows that the de-striping filter effectively suppressed longitudinal stripes to a certain extent. However, it is not sufficient, and so the coefficients need to be further filtered as described in the next section (even the northward component data have to be filtered in the same way).

2.2.2 Fan filter

The best filter to make the spatial distribution of gravity change smooth is the two-dimensional Gaussian filter, called Fan filter [*Wahr et al.*, 1998; *Zhang et al.*, 2009]. The definition of this filter and how to apply it to the coefficients are shown with equations (2.2) ~ (2.6).

$$\Delta g(\theta, \varphi) = \frac{GM}{R^2} \sum_{m=2}^{nmax} (n-1) W_n \sum_{m=0}^{n} W_m (\Delta C_{nm} \cos m\varphi + \Delta S_{nm} \sin m\varphi) \overline{P_{nm}}(\sin\theta) \quad (2.2)$$

$$W_0 = 1 \quad (2.3)$$

$$W_1 = \frac{1+e^{-2b}}{1-e^{-2b}} - \frac{1}{b} \quad (2.4)$$

$$W_{n+2} = -\frac{2n+1}{b} W_{n+1} + W_n \quad (2.5)$$

$$b = \frac{\ln(2)}{(1-\cos\frac{r}{R})} \qquad (2.6)$$

where W_n and W_m are the weighting function with Gaussian distribution at degree *n* and *m*, and *r* is the averaging radius. Weights with different *r* are shown in figure 2.9.

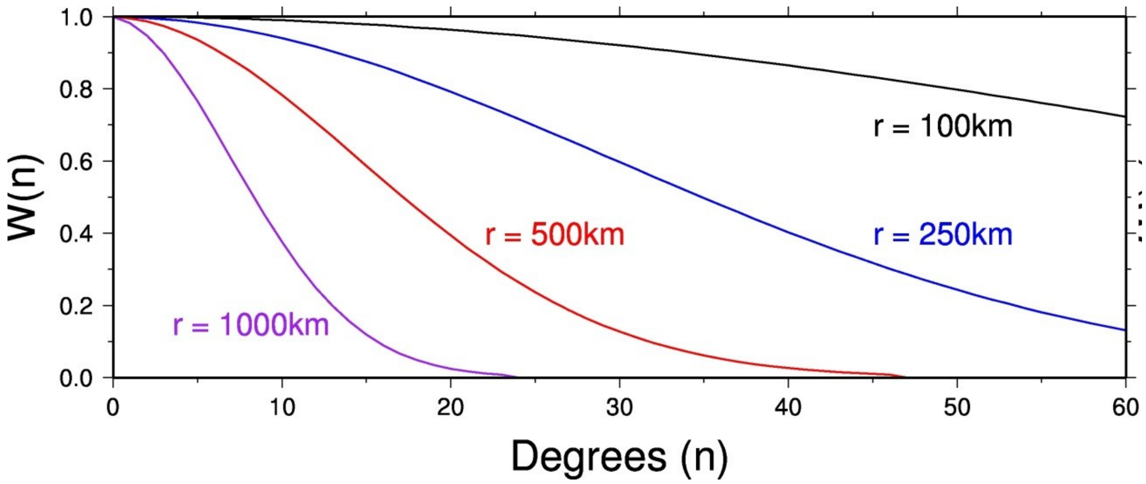

Figure 2.9 The values of *W(n)* as a function of degree *n* for the different values of *r*, i.e. 100 km, 250 km, 500 km, and 1000 km. For larger degrees, the weight becomes smaller.

Figure 2.9 shows that the fan filter gives smaller weights to coefficients of higher degree and order. That is why the shortwave noises are reduced by this filter. The gravity changes from October to November 2013 calculated with GRACE data after the de-striping filter and the fan filter are shown in Figure 2.10.

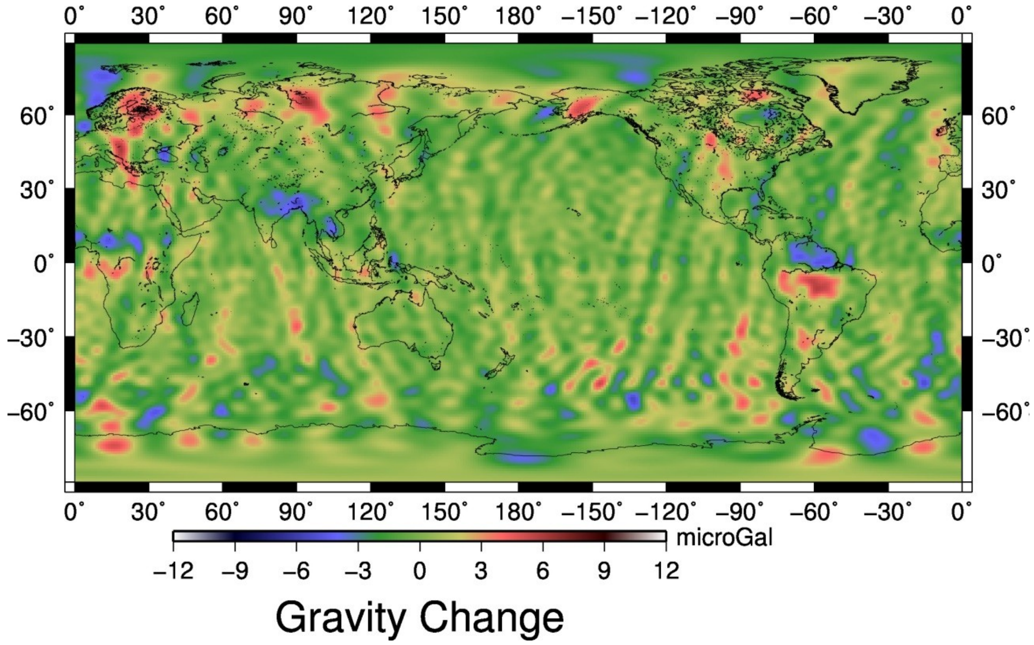

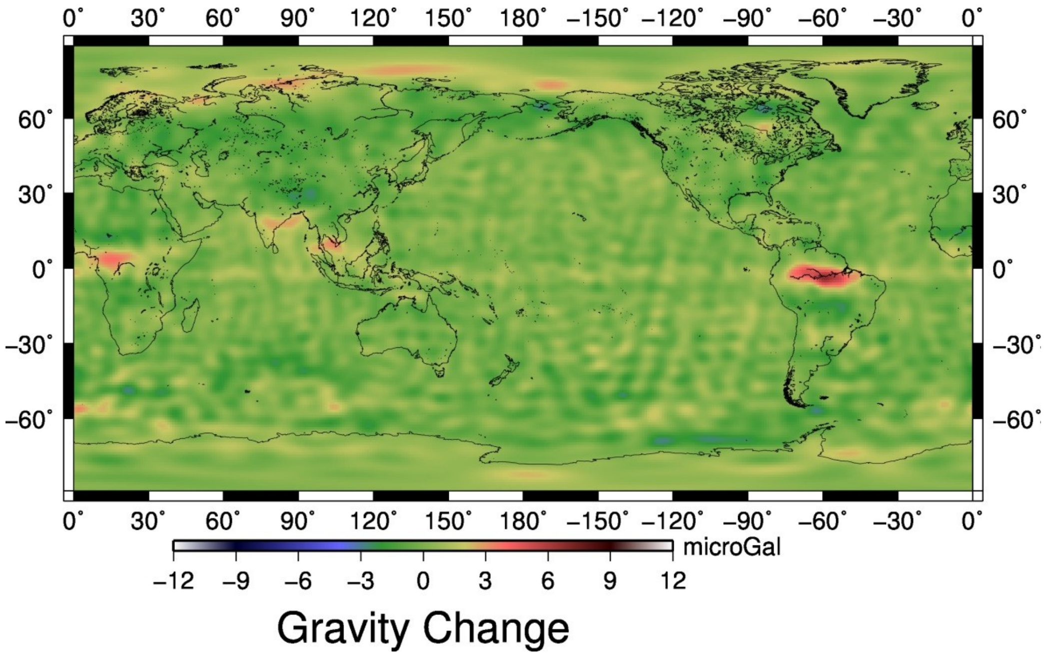

Figure 2.10 The gravity changes from October to November 2013. (above) The downward components of gravity change calculated from GRACE data with both de-striping (P3M15) and Fan filter (r = 250km). (below) The northward components of gravity change calculated from GRACE data with Fan filter (r = 250km).

2.3 GLDAS model

In this study, GLDAS Noah model [*Rodell et al.*, 2004] is used to remove the contribution of land hydrology to gravity. GLDAS model is made from the observed data of precipitation, temperature, and so on, and given as monthly values at 1×1 degree grid points, except for Antarctica and Greenland. The data give the amount of water (kg/m^2) there, so it has to be changed into spherical harmonic coefficients and into those of gravity by formulations given in *Wahr et al.* [1998]. They are filtered in the same way to de-stripe and reduce short-wavelength noises as for the GRACE data. Before converting to spherical harmonic coefficients, grid values in Greenland/Antarctica were set to zero.

2.4 Time series analysis

The function (2.7) is fitted to the GRACE data with the least-squares method to estimate the postseismic gravity changes and the function (2.8) is used to get the time series of gravity deviations by eliminating components not related to earthquakes.

$$G = a + bt + c\,sin(\omega t + \theta_1) + d\,sin(2\omega t + \theta_2) + H(t)\left\{\Delta g + \sum_i e_i \times f_i(\Delta t)\right\} \tag{2.7}$$

$$\hat{G} = G - \{\, bt + c\sin(\omega t + \theta_1) + d\sin(2\omega t + \theta_2)\,\} \tag{2.8}$$

There $f_i\,(\Delta t)$ are certain functions to be fitted to the time-decaying components after the earthquakes and the others in (2.7) are the same as (1.1). $\hat{G}$ is the gravity changes obtained by removing the secular and seasonal components. We will discuss what kind of $f_i(\Delta t)$ best models the postseismic gravity changes in the chapter of results and discussion.

2.5 Model calculation

The software package by *Sun et al.* [2009] is used to calculate coseismic gravity changes together with fault parameters shown in *Banerjee et al.*, [2005] for the 2004 Sumatra-Andaman earthquake, *Heki and Matsuo* [2010] for the 2010 Chile (Maule) earthquake, and *Matsuo and Heki* [2011] for the 2011 Tohoku-oki earthquake.

The contribution of sea water to gravity also has to be added because *Sun et al.* [2009] gives the amount of gravity changes on “dry” earth, which has no water on it. The earthquakes give the surface of the earth deformation and it makes the sea water move, so the observed gravity changes have contributions of both dry earth and sea water. The correction is simply achieved by assuming the gravity field made by thin sea water layer as deep as the vertical crustal movements.

3 Results and discussion

3.1 Re-analysis of postseismic gravity changes of 2004 Sumatra-Andaman earthquake.

We re-analyzed the postseismic gravity changes of 2004 Sumatra-Andaman earthquake with newer data (Release 05) than those used in Ogawa and Heki [2007] (Release 02) with the function (1.1), and found that the gravity had decreased for a few months after the earthquake and increased slowly. This cannot be found from the function (1.1) because the component of the function (1.1) for postseismic gravity changes is only one exponential, which is used for long-term increasing (the red curve in figure 3.1). Then, we gave one more exponential to the function (function (3.1)), and fitted it to both the short- and long-term postseismic gravity changes (the blue curve in figure 3.1). This discovery got us wondering how about gravity changes of other earthquakes and two-dimensional distribution of postseismic gravity changes, so we analyzed the time series of gravity changes of the 2004 Sumatra-Andaman earthquake, 2010 Chile (Maule) earthquake, and 2011 Tohoku-oki earthquake.

$$G = a + bt + c\sin(\omega t + \theta_1) + d\sin(2\omega t + \theta_2)$$
$$+H(t)\left\{\Delta g + e_1\left(1 - \exp\left(\frac{\Delta t}{\tau_1}\right)\right) + e_2\left(1 - \exp\left(\frac{\Delta t}{\tau_2}\right)\right)\right\} \qquad (3.1)$$

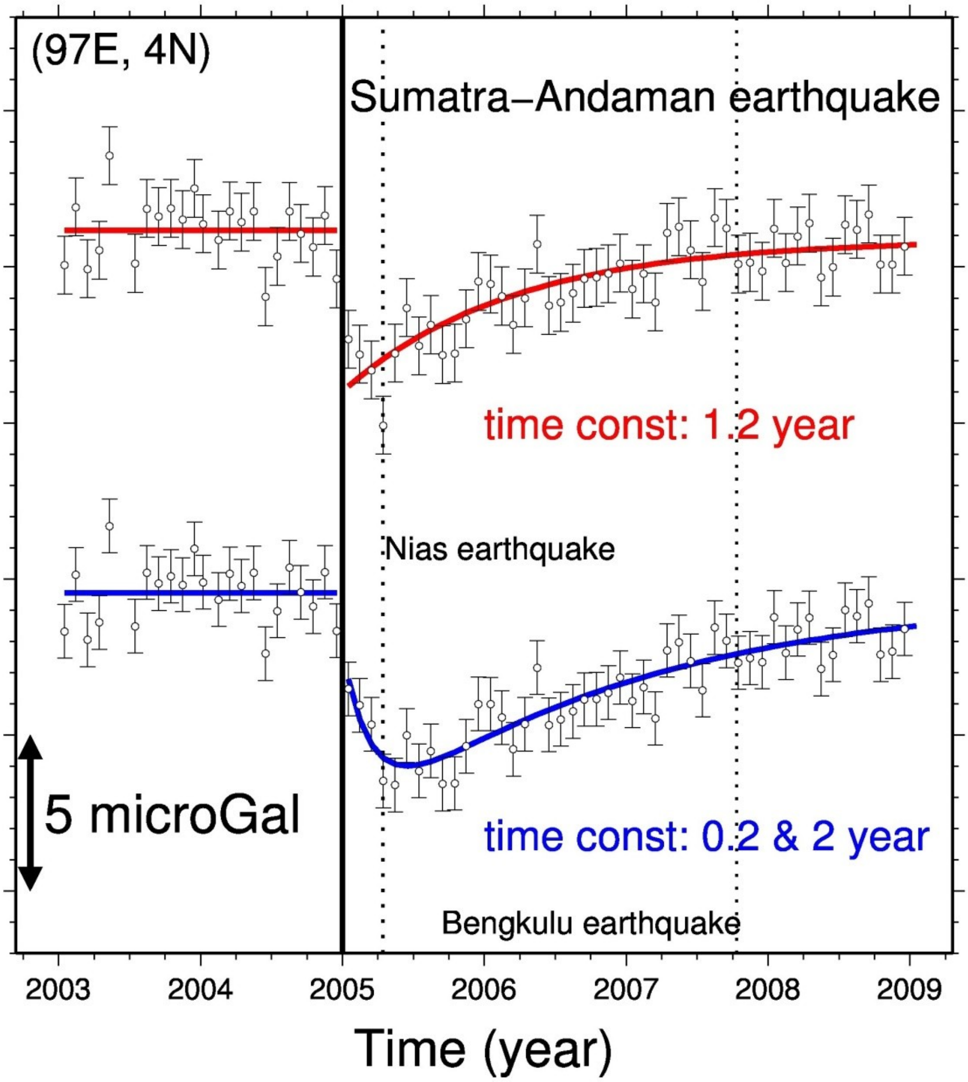

Figure 3.1 Time series of gravity changes before and after the 2004 Sumatra-Andaman earthquake at 4N97E (shown in figure 3.2) fitted with two different models. The white circles are the time series after removing seasonal and secular gravity changes and the steps at the 2005 Nias earthquake and 2007 Bengkulu earthquake. The vertical lines indicate the earthquake occurrences. The red and blue curves are fitted with postseismic change with one component (τ=1.2 year) and with two components (τ_1=0.2 year and τ_2=2 year), respectively. The gravity decrease immediately after the earthquake is well modeled only with the blue curve.

3.2 Co- and postseismic gravity changes of three Mw9-class earthquakes

3.2.1 Downward gravity changes (Observed and calculated)

3.2.1.1 Coseismic gravity changes

In Figure 3.2 we compare the distributions of coseismic, and short- and long-term postseismic gravity changes of the three megathrust events. The signal-to-noise ratio is not good especially for the Maule earthquake due to the relatively small magnitude and large land hydrological signals. In fact, this area is known to have experienced a drought in 2010. The removal of hydrological signals by GLDAS does not work well enough in this region (Figure 3.3) due possibly to insufficient meteorological observations to be input to the GLDAS models. Nevertheless, characteristic gravity signals are seen near the epicenter.

Figure 3.2 (a-1, b-1, and c-1) shows that the coseismic signatures of the three cases are dominated by gravity decreases on the back arc side of the fault with smaller increases on the fore arc side. The latter are often attenuated by the existence of seawater [*Heki and Matsuo*, 2010]. Such coseismic changes are well understood with the theory discussed in section 1.3. The signature of the latter after spatial filtering, and appears as the gravity decrease on the back arc side of the arc [*Han et al.*, 2006].

The results of model simulation are shown in Figure 3.5 ~ 3.7, calculated with the method in the section 2.5. Each of them has difference between the result of observation and that of calculation but the gravity changes are observed well to some extent; our results are pragmatic.

3.2.1.2 Postseismic gravity changes

The middle column of Figure 3.2 suggests that the short-term postseismic gravity changes also show negative polarities, although their centers seem to shift from back-arc regions toward trenches. On the other hand, the long-term postseismic gravity changes (the right column of Fig.3.2) have positive polarities and occur directly above the ruptured fault. These features are common in the three earthquakes.

The elastic response to the afterslip should occur as the continuation of the coseismic gravity changes. The distribution of the postseismic gravity changes by the afterslip of the 2011 Tohoku-oki earthquake is shown in Figure 3.8, which was calculated with the software of Sun et al. [2009] from the afterslip distribution shown in Figure 3.9 calculated from GPS data. They are both dominated with negative changes. However, the trenchward shift of the center exists, and this cannot be explained simply by the slip distribution difference (center of afterslip is shifted down-dip from that of the main shock [*Ozawa et al.*, 2012]). In addition to that, the time constant of the short-term postseismic gravity change of the 2011 Tohoku-oki earthquake (0.1 year) is different from the afterslip (0.4 year in Ozawa et al. [2012], but the mathematical model is different from ours).

The long-term postseismic gravity changes may reflect multiple processes except for afterslip. So far, several mechanisms have been proposed for the postseismic gravity changes, e.g. viscous relaxation of rocks in the upper mantle [*Han and Simons*, 2008; *Panet et al.*, 2007; *Tanaka et al.*, 2006; *Tanaka et al.*, 2007], diffusion of supercritical water around the down-dip end of the ruptured fault [*Ogawa and Heki*, 2007].

The viscoelastic mantle relaxation can play the main role of long-term postseismic gravity change. Figure 3.10 shows the postseismic gravity changes for two years from observation and from calculation on viscoelastic postseismic deformation with the method of Tanaka et al. [2006] and Tanaka et al. [2007]. This figure suggests that the mantle relaxation has the strong possibility to explain postseismic gravity changes. However, this does not disprove other possibilities and also has a problem that the viscoelastic relaxation takes a long time (10 years or more generally) because of the big viscosity of rocks in mantle. The averaging viscosity in the upper mantle at ~100km is more than 10^20 (Pa sec) [*Fei et al.*, 2013] and the calculation results take 3×10^18 (Pa sec). This small viscosity has to be taken to explain the long-term postseismic gravity changes with the viscoelastic mantle relaxation. Even if the mantle under the faults of 2004 Sumatra-Andaman earthquakes are much softer than the average, the long-term postseismic gravity changes of 2010 Chile (Maule) earthquake and 2011 Tohoku-oki earthquake take only a few months to get increased. It is not very natural that all of the viscosities of the rocks under the faults of the three megathrust earthquakes are much lower than average. Viscoelastic mantle relaxation has strong possibility that it plays an important role of long-term postseismic gravity changes but it cannot explain them completely.

The diffusion of supercritical water around the down-dip end of the ruptured fault can explain the postseismic gravity increase in this timescale to some extent, but there have been no decisive evidence to prove or disprove it. And there is another problem: both of viscoelastic relaxation and diffusion of supercritical water do not explain the distribution of the changes, i.e. they occur directly above the rupture area.

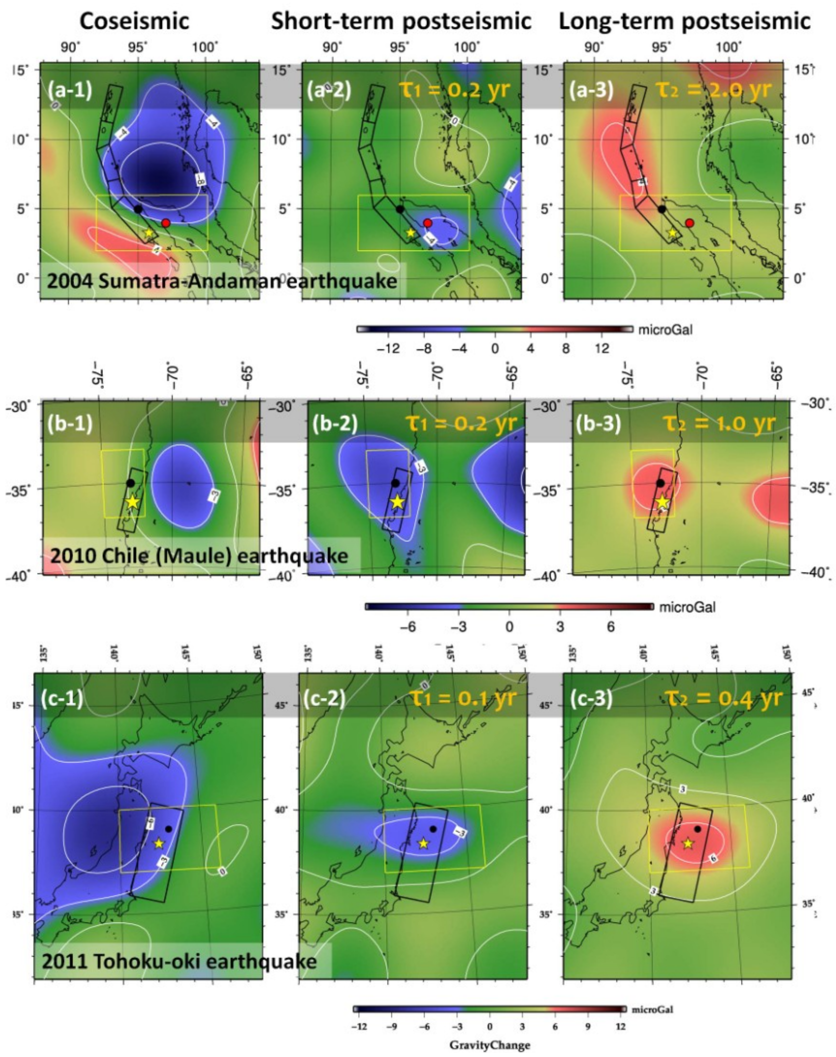

Figure 3.2 Coseismic (left), and short-term (middle) and long-term (right) postseismic gravity changes of the three M9 class earthquakes, i.e. the 2004 Sumatra-Andaman (a), the 2010 Maule (b), and the 2011 Tohoku-Oki (c) earthquakes. The postseismic gravity changes are expressed with 2 year (the 2004 Sumatra-Andaman) and 1 year (the other two earthquakes) cumulative changes. Time constants are shown on the figure. The yellow stars and black squares show the epicenters and the approximate outlines of the faults that slipped in the earthquakes. The red circles in (a) and the black circles in in (a), (b), and (c) show the points whose gravity time series are shown in Figure 3.1 (red circles) and in Figure 3.4 (black circles). The yellow squares show the areas whose data are used for F-test in section 3.2.2. The contour intervals in (a), (b), and (c) are 4 μGal, 3 μGal, and 3 μGal, respectively. The gravity show coseismic decreases, then keep decreasing for a few months (short-term postseismic). It then increases slowly (long-term postseismic) with slightly different spatial distribution from the other two components.

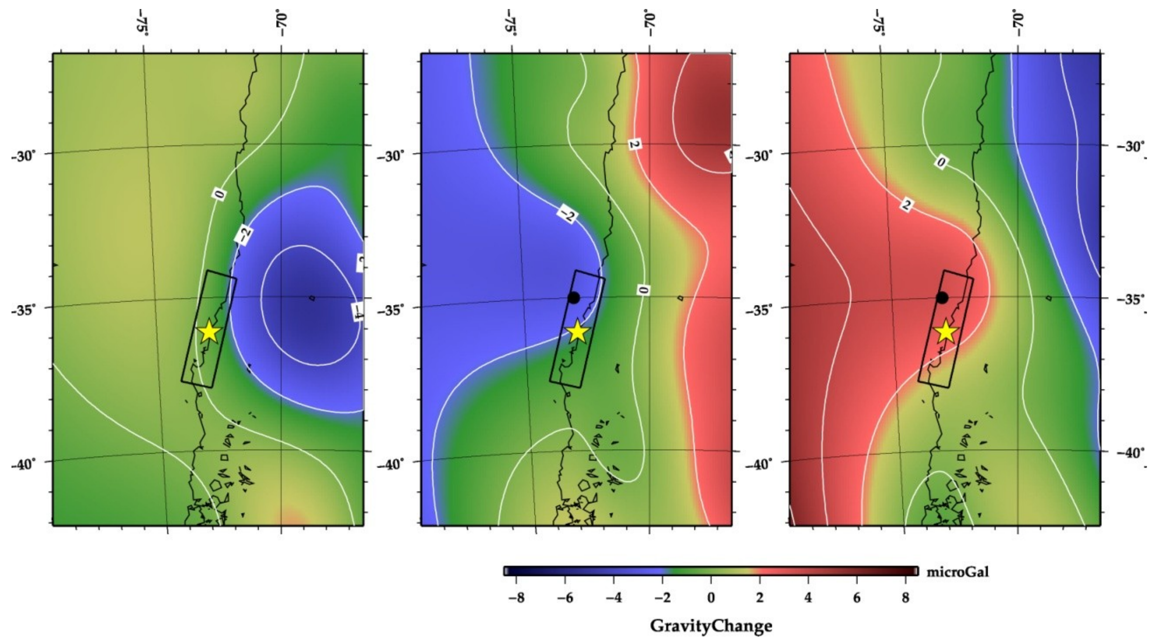

Figure 3.3 Co- (left) and postseismic (middle and right) gravity changes calculated with GRACE data and GLDAS model. GLDAS model gives noises to short- and long-term (middle and right) gravity changes.

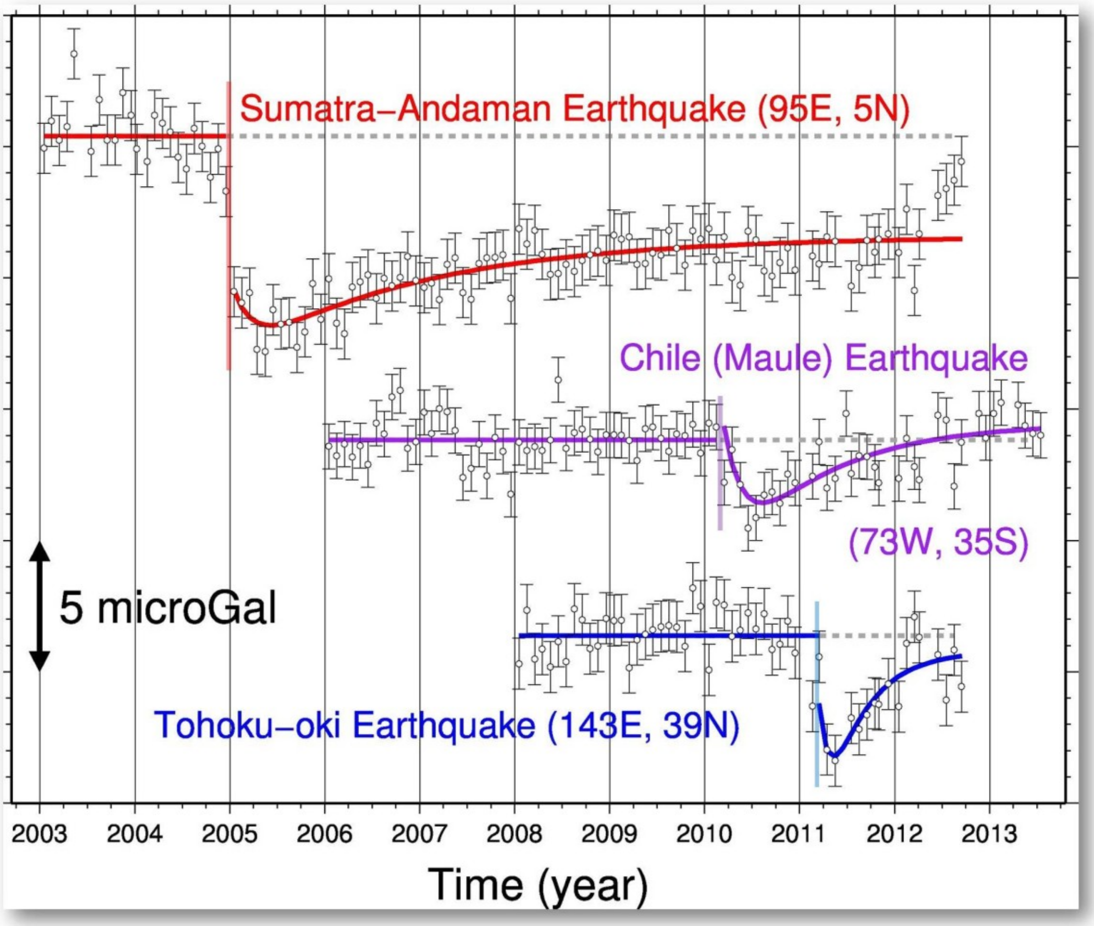

Figure 3.4 Time series of gravity changes before and after the three megathrust earthquakes at the black circles shown in Figure 3.2. The white circles are the data whose seasonal and secular changes were removed. The vertical translucent lines denote the earthquake occurrence times. All the three earthquakes suggest the existence of two postseismic gravity change components with two distinct time constants.

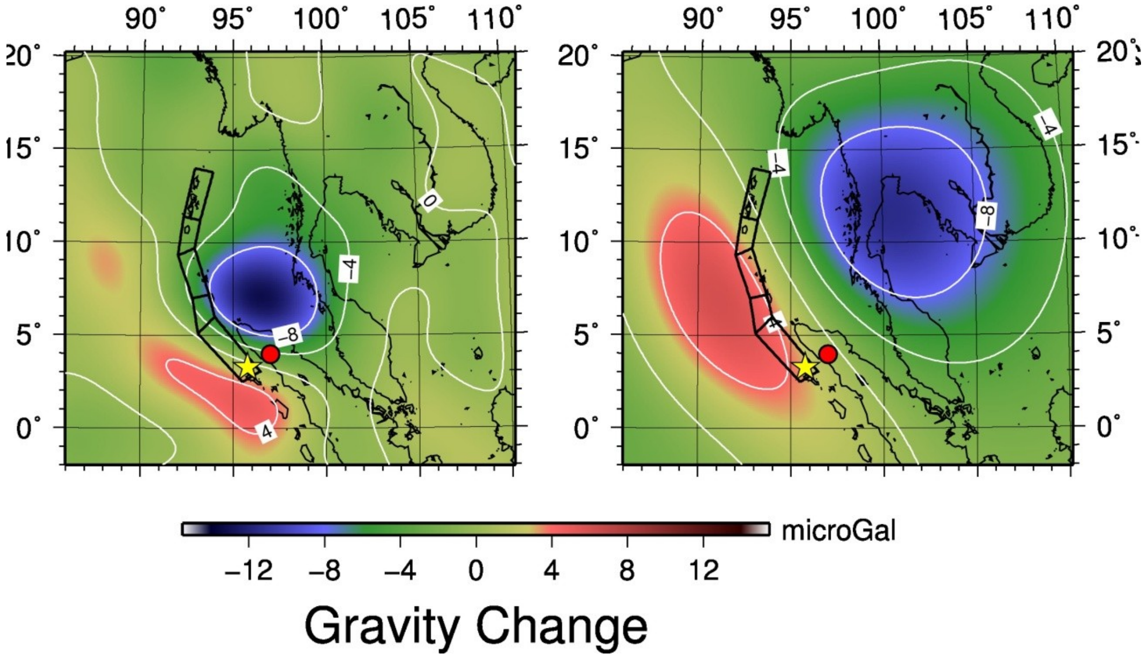

Figure 3.5 The distribution of observed coseismic gravity change of 2004 Sumatra-Andaman earthquake (left) and that of calculated with the software of Sun et al. [2009] and the fault model of Banerjee et al. [2005] (right) as section 2.5. The amount of gravity changes are near each other but the spatial pattern is completely different. This may be because the fault model is not so good to explain the coseismic gravity change.

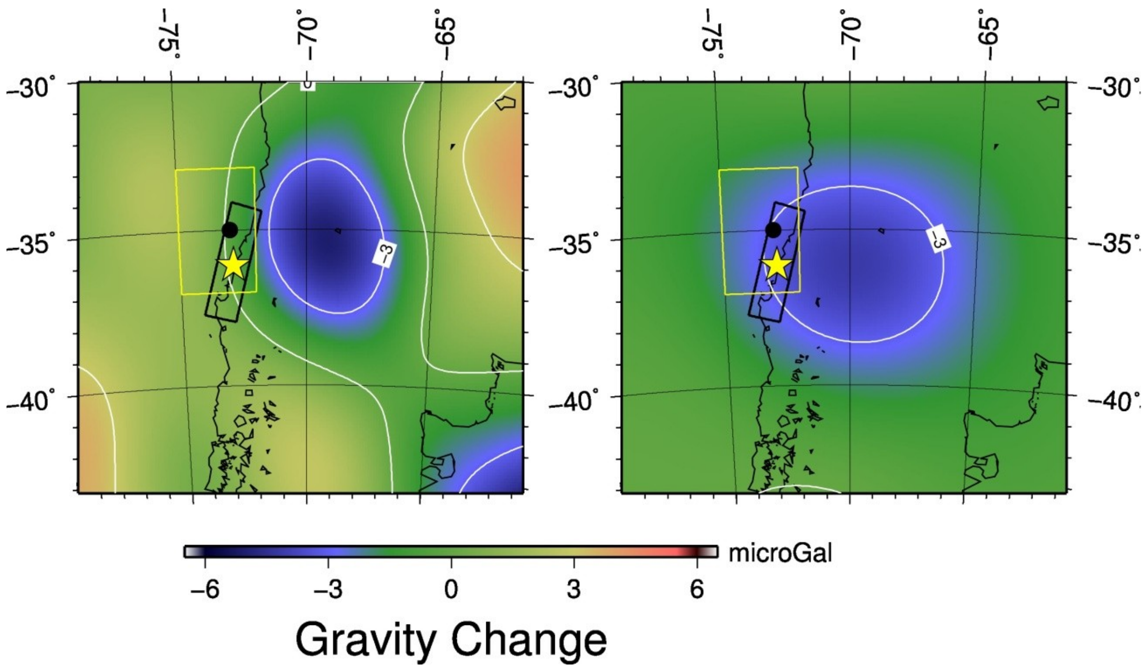

Figure 3.6 The distribution of observed coseismic gravity change (left) of 2010 Maule

earthquake and that of calculated with the software of Sun et al. [2009] and the fault model shown in Heki and Matsuo. [2010] (right) as section 2.5. The left figure and right one is similar to each other. The yellow squares, black squares, yellow stars, and black points are the same as Figure 3.2.

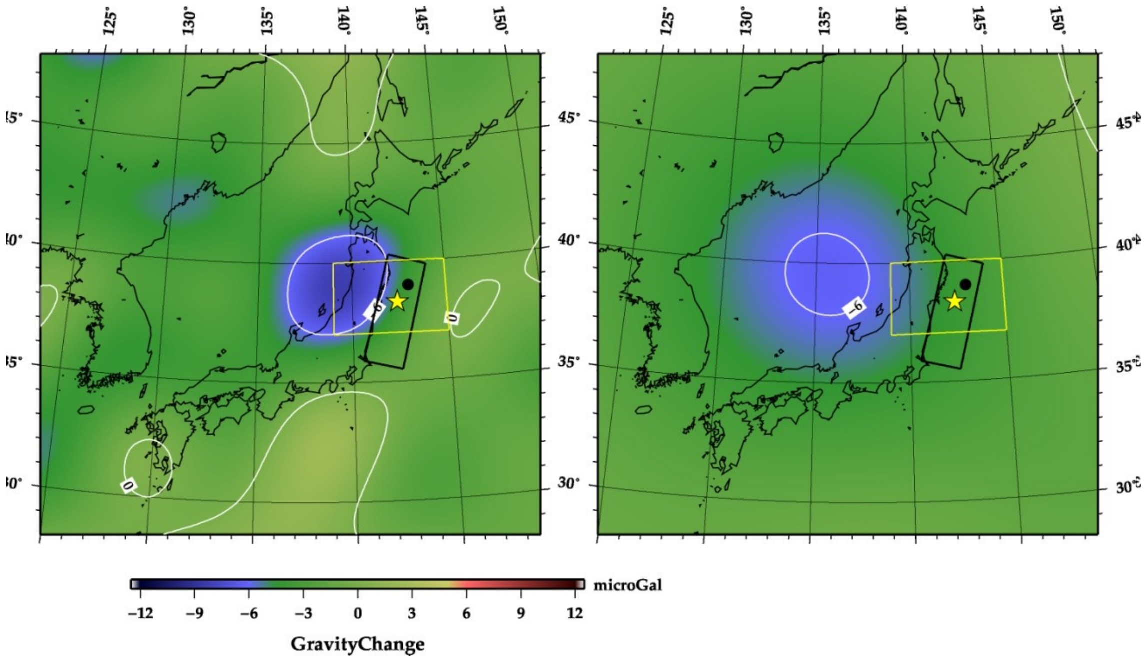

Figure 3.7 The distribution of observed coseismic gravity change (left) of 2011 Tohoku-oki earthquake and that of calculated with the software of Sun et al. [2009] and the fault model shown in Matsuo and Heki [2011] (right) as section 2.5. The left figure and right one is similar to each other to some extent. The yellow squares, black squares, yellow stars, and black points are the same as Figure 3.2.

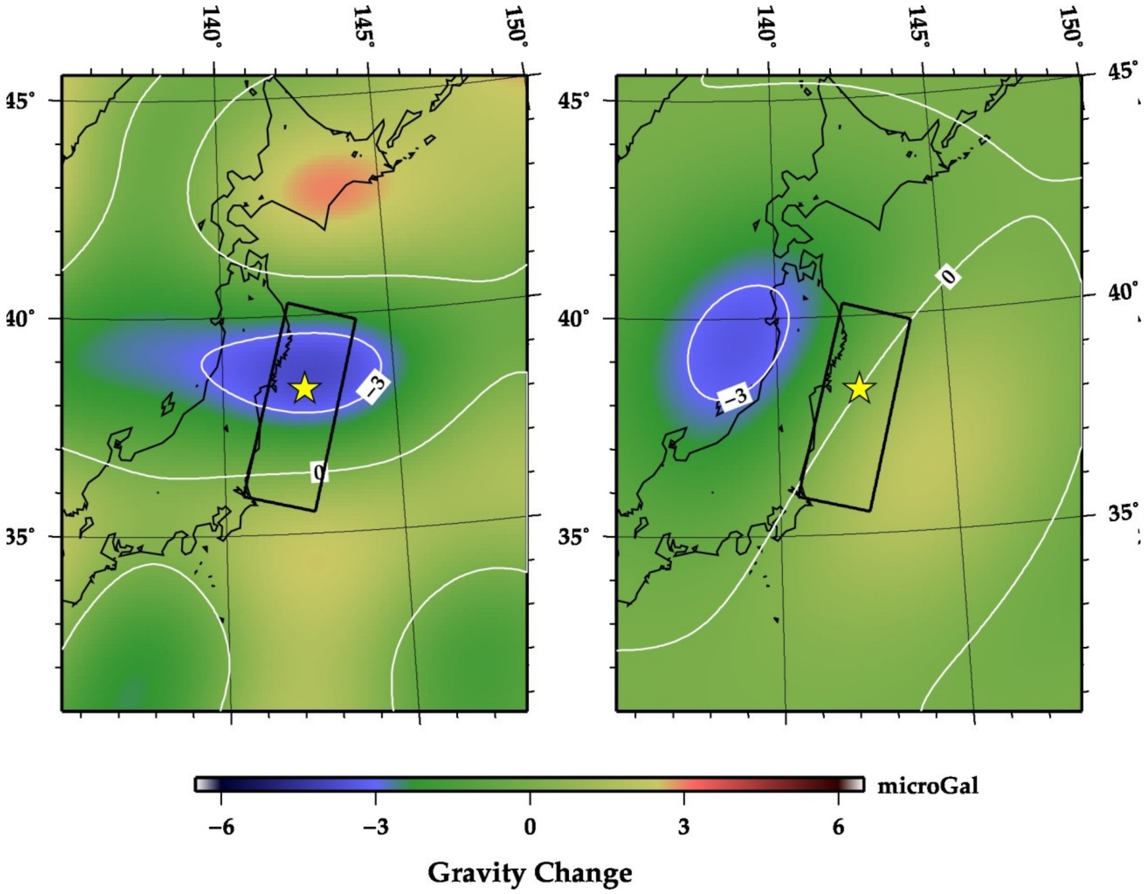

Figure 3.8 (left) The same figure as (c-2) of figure 3.2. (right) The gravity changes of the afterslip calculated with the slip distribution from GPS data shown in Figure 3.9 by Dr. Matsuo. The amounts of gravity changes are near but spatial patterns are different.

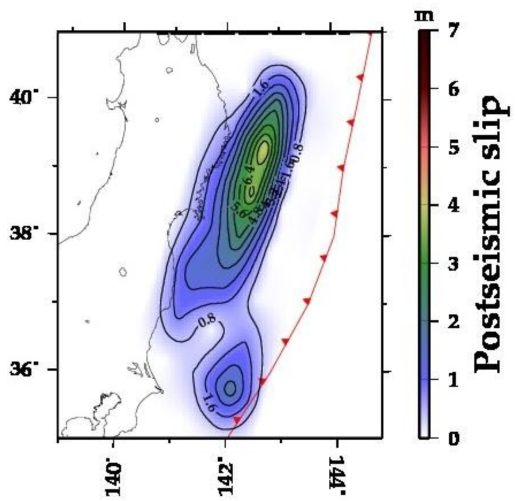

Figure 3.9 The slip distribution of the afterslip of 2011 Tohoku-oki earthquake calculated from GPS data.

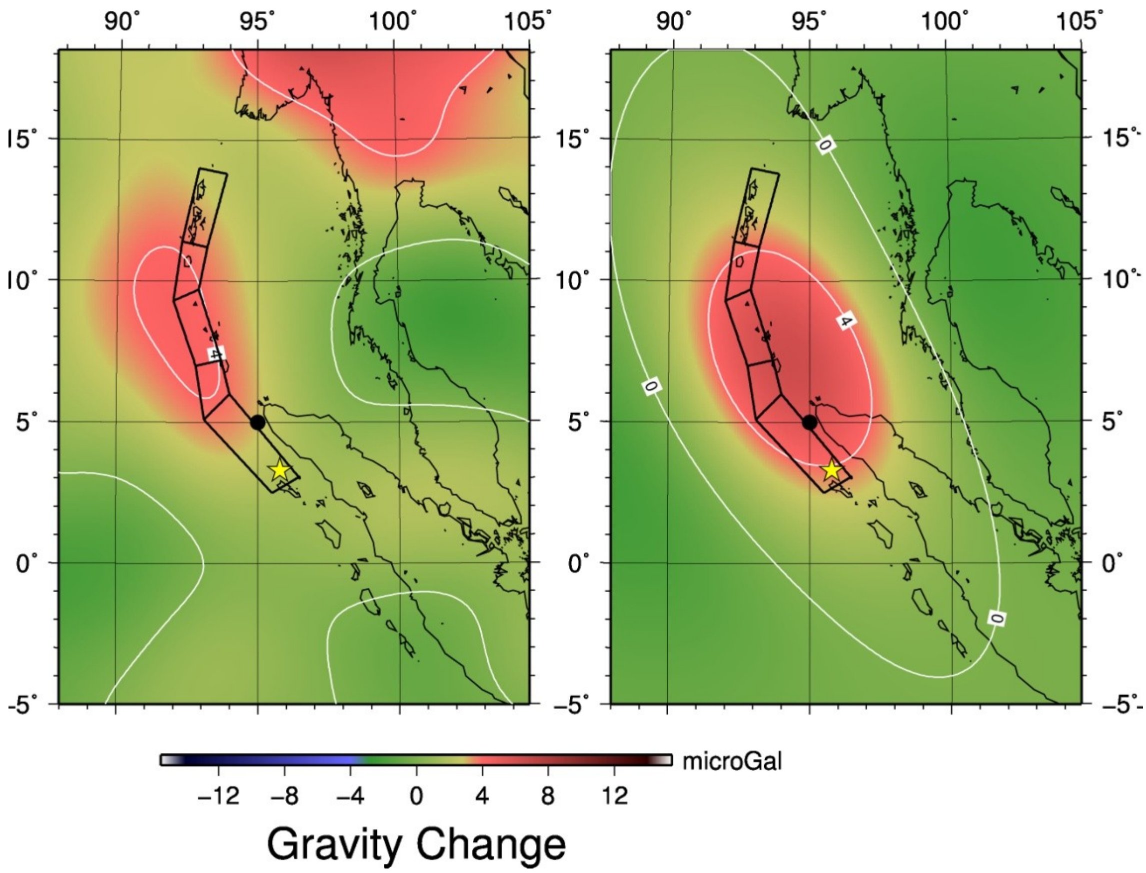

Figure 3.10 (left) The same figure as (a-3) of figure 3.2. (right) The gravity changes of the viscoelastic mantle relaxation calculated with the viscosity = 3×10^18 (Pa sec) by Prof. Tanaka at Tokyo University, with the method of Tanaka et al. [2006] and Tanaka et al. [2007]. Both of the amounts and spatial patterns of gravity changes are very similar.

3.2.2 F-test

The F-test is done to deny that signals are actually noises. The F-test is a statistical hypothesis tests to get the possibility of coincident of two groups, so the possibility that two groups are different is high when the possibility of F-test is low. This test is done with below formulas (3.2) ~ (3.5).

At first, the short-term postseismic gravity changes are presumed to be noises. Then each data becomes independent because they are just noises, so F-test can be done. If the results of F-test say the possibilities of coincidence are high, the hypothesis that they are noises is affirmed. But the possibilities are low, the hypothesis is denied and the short-term gravity changes are actually signals.

I estimated the difference of variances when the number of exponential components is one and two with the data within yellow squares in Figure 3.2 for two months after the earthquake to do F-test.

$$\sigma^2 = \frac{\sum(x-\bar{x})^2}{n-1} \tag{3.2}$$

$$F = \frac{variance\ 1}{variance\ 2} = \frac{\sigma_1^2}{\sigma_2^2} \tag{3.3}$$

$$f(F, \emptyset_1, \emptyset_2) = \left(\frac{\emptyset_1}{\emptyset_2}\right)^{\frac{\emptyset_1}{2}} \frac{\Gamma(\frac{\emptyset_1+\emptyset_2}{2})}{\Gamma\left(\frac{\emptyset_1}{2}\right)\Gamma\left(\frac{\emptyset_2}{2}\right)} \frac{F^{\frac{\emptyset_1-2}{2}}}{\left(1+\frac{\emptyset_1}{\emptyset_2}F\right)^{\frac{\emptyset_1+\emptyset_2}{2}}} \tag{3.4}$$

$$\Gamma(z) = \int_0^{\infty} t^{z-1}e^{-t}dt \tag{3.5}$$

Where σ^2 = variance (σ = standard deviation), x = values of data, $\bar{x}$ = the mean of x, n = total number of x, $\emptyset$ = flexibility of the data (= n – 1), and Γ is the gamma-function (e is the exponential). The f gives the possibility that the difference of variances of two groups is insignificant. In this study, x is an observed gravity value and $\bar{x}$ is a value of the fitted function..

Each time constant for the function with single exponential is decided so that the variance of whole data gets the least (Figure 3.11). But time constants for the function with double exponential cannot be decided in this way because the short- and long-term postseismic gravity changes with the time constants taken in that way become much larger than coseismic gravity changes in both terms of amounts and spatial distributions of gravity changes (Figure 3.12). Though the mechanisms of postseismic gravity changes are not clear, this is unreasonable obviously. The double time constants are decided so that the functions fit the data near the epicenters well visually. Although this is not the greatest method and should be improved, the result of F-test also shows that postseismic gravity changes have two components.

Earthquake	Time constants (yr)	*n*	*Variance*	Possibility of coincidence
2004 Sumatra-Andaman	1.1	90	1.11079	1.3 × 10^(-27)
	0.2 & 2.0		0.08579	
2010 Chile (Maule)	10^7	40	2.39388	9.4 × 10^(-3)
	0.2 & 1.0		1.13140	
2011 Tohoku-oki	1.0	56	0.51032	6.2 × 10^(-3)
	0.1 & 0.4		0.25755	

Table 3.1 The results of F-test. The possibilities of coincidence are very small. The difference between the results of single-exponential-function fitting and double-exponential-function fitting is significant.

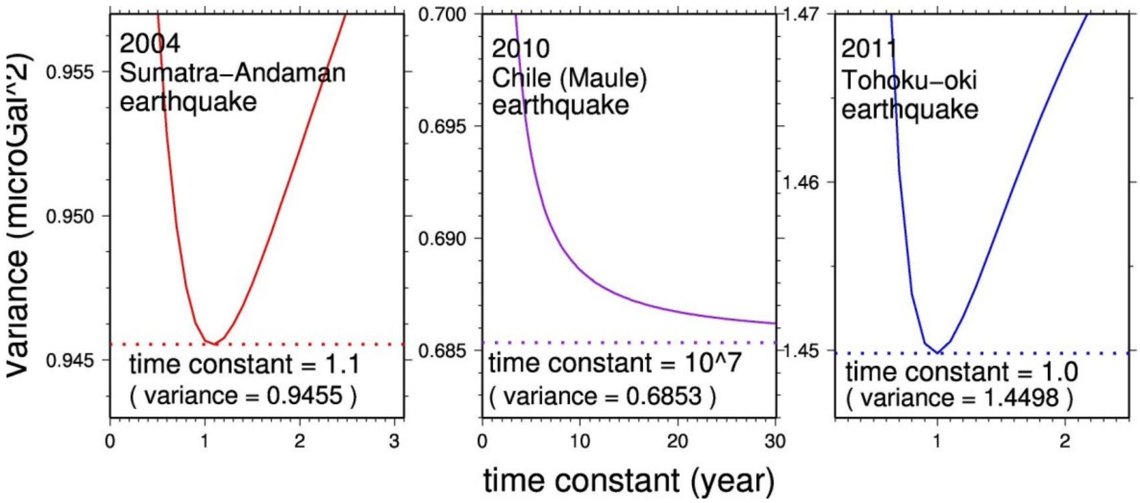

Figure 3.11 Variances (the whole of observed gravity data after the earthquakes) and time constants.

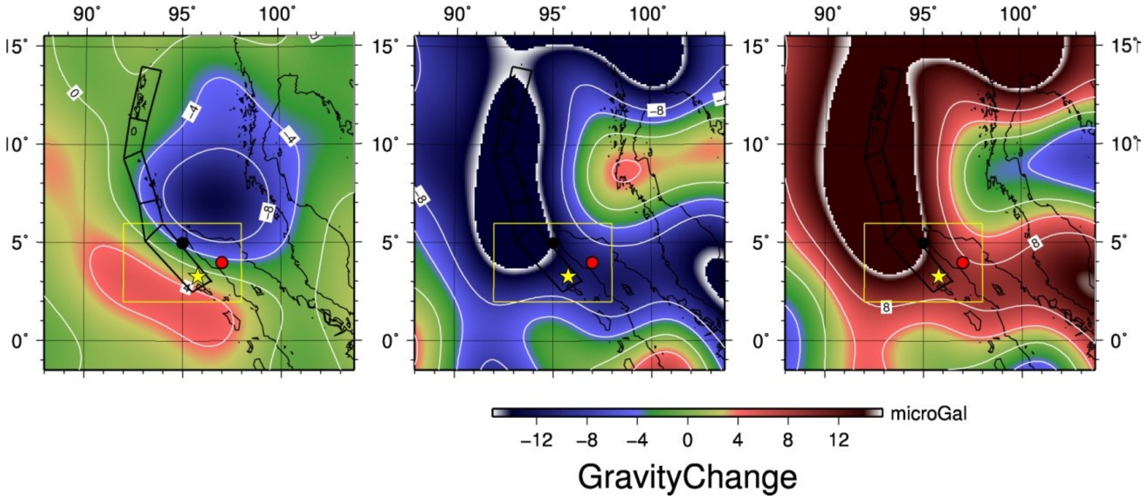

Figure 3.12 The gravity changes calculated with the time constants of 0.3 year and 0.4 year, which gives the least variance. The all marks are the same as Figure 3.2. This figure shows that the method of getting the least variance (or RMS) cannot be used to get two time constants.

3.2.3 Northward gravity changes (Observed)

The northward co- and postseismic gravity changes are also calculated from the GRACE data with the Fan filter (r = 250km) and without de-striping filter. They are shown in Figure 3.13 ~ 3.20. Coseismic gravity changes have northward components but postseismic gravity changes are not clear and there are no significant difference of the variances between the single-component fittings and the double-components fittings. This does not prove nor disprove that postseismic gravity change has two components.

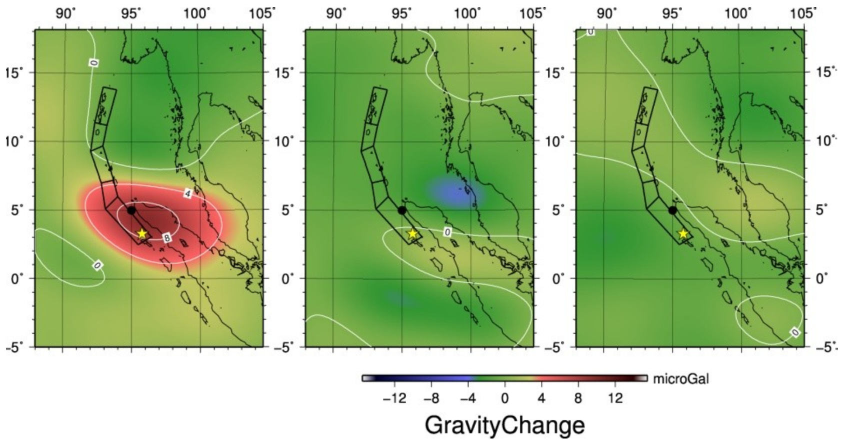

Figure 3.13 The co- (left) and postseismic (middle and right) northward gravity changes of 2004 Sumatra-Andaman earthquake. The all marks are the same as figure 3.2. The coseismic gravity change is very big and large but postseismic gravity changes are not seen well.

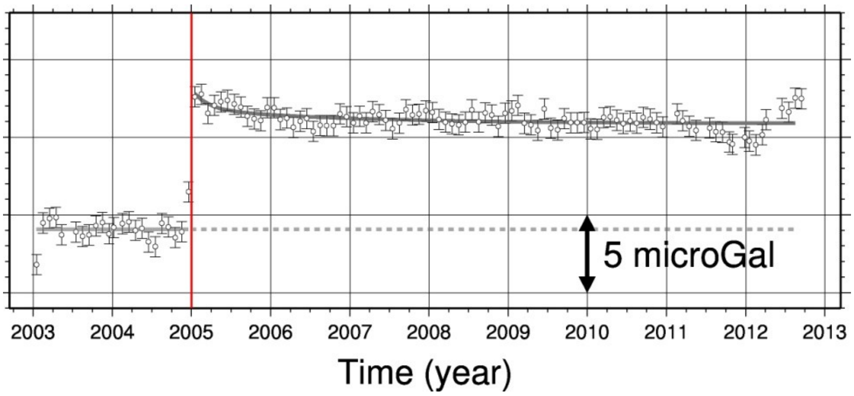

Figure 3.14 The time series of northward gravity changes of 2004 Sumatra-Andaman earthquake at the black point in Figure 3.13 (95E, 5N). The gravity decreased a little after the earthquake, but the second component is not seen in this time series.

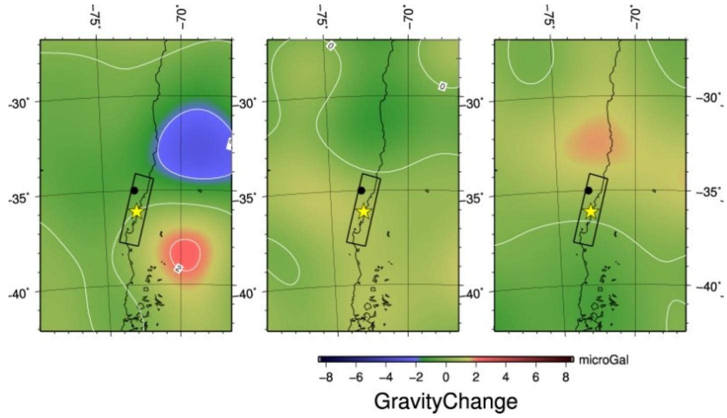

Figure 3.15 The co- (left) and postseismic (middle and right) northward gravity changes of 2010 Chile (Maule) earthquake. The all marks are the same as figure 3.2. The coseismic gravity change is seen but postseismic gravity changes are not.

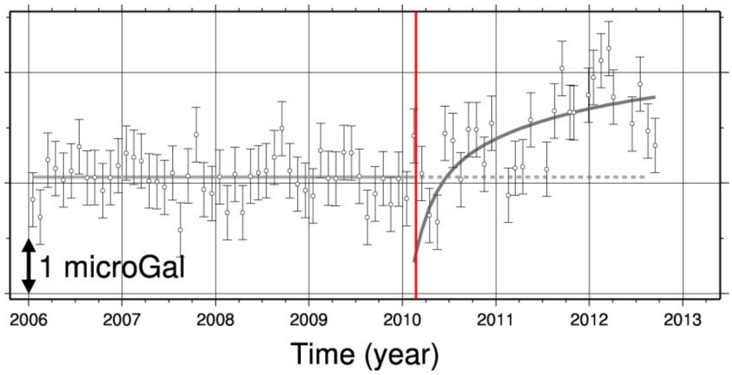

Figure 3.16 The time series of northward gravity changes of 2010 Chile (Maule) earthquake at at the black point in Figure 3.15 (75W, 35S). Postseismic gravity change is seen well but this is not seen in Figure 3.15 because the both of double components are used to fit the curve to the data.

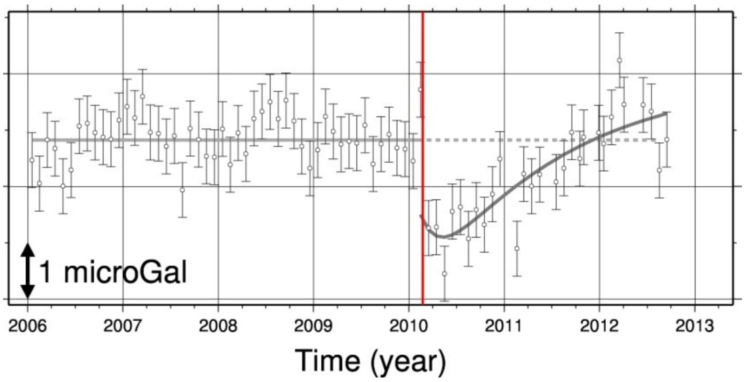

Figure 3.17 The time series of northward gravity changes of 2010 Chile (Maule) earthquake at at (72W, 33S), on the light red in Figure 3.15 (right). The gravity decreased for a few months after the earthquake and increased for longer period, but this is not enough to say there is significant difference.

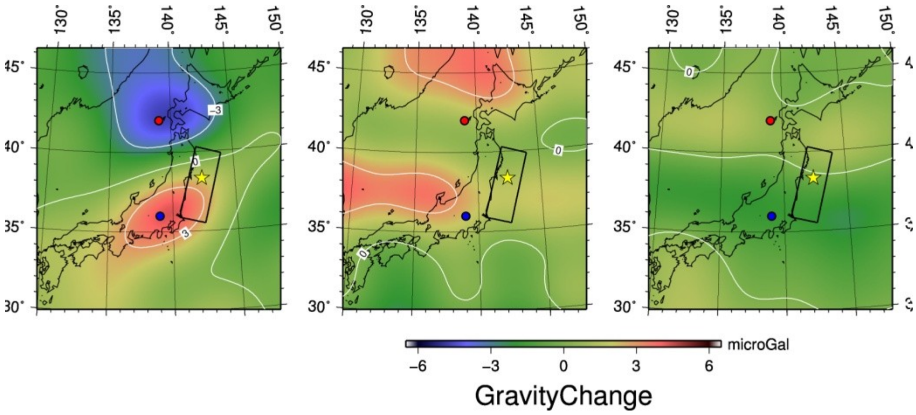

Figure 3.18 The co- (left) and postseismic (middle and right) northward gravity changes of 2011 Tohoku-oki earthquake. The all marks are the same as figure 3.2. The coseismic gravity change is seen but postseismic gravity changes are not. The middle figure is very noisy.

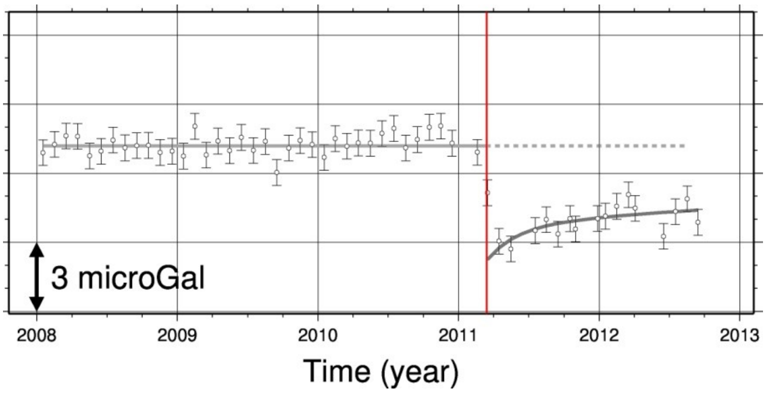

Figure 3.19 The time series of northward gravity changes of 2011 Tohoku-oki earthquake at the red point in Figure 3.18 (139E, 42N). The second component of the postseismic gravity change is not seen in this time series.

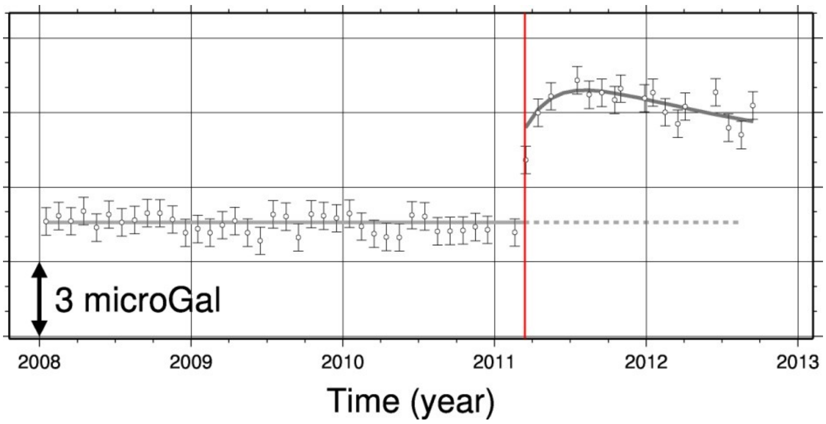

Figure 3.20 The time series of northward gravity changes of 2011 Tohoku-oki earthquake at the blue point in Figure 3.18 (139E, 36N). Two components of the postseismic gravity change are seen well but the possibility of the noise is not disproved because the middle figure in Figure 3.18 is very noisy.

3.3 Contributions of the results

This study suggests that the gravity is the first method to separate phenomena which happen after earthquakes. Main shocks of earthquakes are observed with seismographs and coseismic slips are observed with GNSS, but postseismic phenomena, like afterslip and mantle relaxation, have not been separated with any methods. In this study, that the two components of postseismic phenomena give the gravity changes with different polarities is discovered. This suggests that the gravity measurements can separate them first.

To understand postseismic phenomena is important to understand the physical processes of earthquakes and may be important to predict when and where earthquakes occur because the causes of postseismic phenomena are co- or preseismic phenomena. This study will give the quest for knowledge advance.

4. Summary

Gravity is the third method to observe earthquakes after the seismographs and GNSS. The data of GRACE satellites, which keep on observing the gravity field of the earth, give us the insight into phenomena under the ground and tell us two-dimensionally what happens when and after earthquakes occur.

In this study, the gravity changes of the three mega-thrust earthquakes (2004 Sumatra-Andaman earthquake, 2010 Chile (Maule) earthquake, and 2011 Tohoku-oki earthquake, which occurred after 2002, when the GRACE satellites were launched) are observed with the GRACE and an important fact is found. It is that the gravity which decreases coseismically keeps on decreasing for a few months and increases for a longer period; the postseismic gravity change has two components (short- and long-term gravity changes). It is also supported by F-test. The results of F-test say that the curves fitted to the observed data become much better when it gets the second exponential than when it has only one exponential. Although the northward postseismic gravity changes observed with GRACE do not show the second components, it is clear that the postseismic gravity changes have two components.

The mechanisms of short- and long-term postseismic gravity changes are explained with afterslip and viscoelastic mantle relaxation to some extent but they also have some problems. Afterslip has a problem of spatial pattern. The result of calculation of afterslip gives the good amount of gravity changes and the good spatial scale (size) which explain the observed results well, but does not give a great spatial distribution to explain the observed results. Viscoelastic mantle relaxation has a temporal problem. The good results which explain observation well take much lower viscosity in the mantle than average. Even if the mantle under the faults of 2004 Sumatra-Andaman earthquakes are very soft, the long-term postseismic gravity changes of 2010 Chile (Maule) earthquake and 2011 Tohoku-oki earthquake take only a few months to get increased. It is not very natural that all of the viscosities of the rocks under the faults of the three megathrust earthquakes are very low. Then, other mechanisms may be needed to explain the postseismic gravity changes.

Although the mechanisms of postseismic gravity changes have to be discussed more in the future, the gravity observation as the third sensor for earthquakes gets the postseismic phenomena separated, which the first (seismographs) and second (GNSS and SAR) sensors cannot do. This result gives the quest for knowledge advance.

5. Acknowledgement

I have many people whom I would like to give gratitude and the first person must be Professor Kosuke Heki, my supervisor. I am sure that I could not do my study without him. He gives me warm eyes, many advices to break the walls that I get, many chances to take part in many scientific meetings and to discuss with scientists at other research institutions, jobs as a teaching assistant to solve my economic problems, and many other things which I got with a lot of gratitude. My gratitude to him is beyond description. I am proud that I am a student of him. I will also try to give him something for him and his study while I am at doctor course. Next, I would like to express my gratitude to Dr. Koji Matsuo, who was a senior student at our laboratory and is a postdoctoral researcher at Kyoto University. He also gave me many advices and told me how to use data especially when I was an undergraduate student and a master-course-first-grade student because we studied in the same room and with the same data. Those great helps always got my study much better. I would also like to say thanks to Prof. Yoshiyuki Tanaka at Tokyo University. He gave me the data of Figure 3.10 (right) and explained the theory I had to understand. This was a very big help for my study. I am also grateful to the teachers and students at the solid seminar in Hokkaido University. The teachers also gave me very suggestive advices and comments about my study when I made my presentation, which got my study advanced again and again. The students gave me a happy and exciting life in laboratory. And knowing what and how teachers and other students study in our seminar gets me excited very much. I am happy that I am going to be a doctor course student in this environment.

謝辞

本研究は，多くの方々の協力を賜って達成しました．ここにその謝辞を記します．

第一に，指導教官の日置教授に感謝を示したく思います．日置教授は私を見守ってくださり，時には私のつまずきを打破する助言をくださり，時には様々な学会や勉強会に参加して色々な研究者の方々と議論する機会を与えてくださり，また時にはティーチング・アシスタントの仕事を紹介してくださり，本当に様々な面で良くしていただきました．この感謝を示す適切な言葉を見つけようとしましたが，どうやらそれは私の能力を超えているようです．ただ，本当にありがとうございました．日置教授が指導教官で良かったと思っています．私は更に博士課程に進学いたしますが，そこでは私も教授の研究に貢献できるようなことをしたいと思います．今後ともよろしくお願いします．

次に，この研究室の先輩であり，現在は京都大学で研究者をしていらっしゃる松尾功二さんにお礼を申し上げます．特に私が修士 1 年だった昨年と，学部生だった一昨年は，同じ部屋で同じデータを使って研究していることもあり，多くの助言とご指導をいただきました．その助言とご指導が無ければ，私の研究がどうなっていたのか分からないほどです．厚くお礼申し上げます．ありがとうございました．

また，東京大学地震研究所の助教授である田中愛幸さんにもお礼申し上げます．本研究の図 3.10（右）の結果は田中さんの計算結果を頂いたものであり，私が学ぶべき理論について説明していただくこともありました．観測データを解析するだけでなく，理論を学ぶことも非常に重要であり，その大きな助けをいただくことができました．

更に，私が所属している北海道大学の固体系ゼミの先生方，そして先輩方，同期，後輩の皆様に，ここでお礼を述べさせていただきます．先生方には，私の発表のときに大変有益なお言葉をいただき，それは私の研究を推し進める力になってくれました．また，研究室の生活が豊かなものになったのは，先輩方や同期，更には後輩の皆様のおかげです．ゼミで先生方や他の学生が一体どんな研究を，どのように行なっているのかを聞くと，とてもワクワクしました．この環境で博士課程に進めることを嬉しく思います．

皆様，本当にありがとうございました．これからもよろしくお願いします．

6. References

Banerjee, P., F. F. Pollitz, and R. Bu¨ rgmann, 2005: The size and duration of the Sumatra-Andaman earthquake from far-field static offsets, *Science, 308, 1769 – 1772* doi: 10.1126/science.1113746

Chen, J. L., C. R. Wilson, B. D. Tapley, and S. Grand 2007: GRACE detects coseismic and postseismic deformation from the Sumatra-Andaman earthquake, *Geophys. Res. Lett., 34, L13302,* doi:10.1029/2007GL030356

Fei, H., M. Wiedenbeck, D. Yamazaki, T. Katsura, 2013: Small effect of water on upper-mantle rheology based on silicon self-diffusion coefficients, *Nature,* doi:10.1038/nature12193

Han, S.-C., and F. J. Simons (2008), Spatiospectral localization of global geopotential fields from the Gravity Recovery and Climate Experiment (GRACE) reveals the coseismic gravity change owing to the 2004 Sumatra-Andaman earthquake, *J. Geophys. Res., 113*, B01405, doi:10.1029/2007JB004927.

Han, S.C., Shum, C.K., Bevis, M., Ji, C., Kuo, C.Y., 2006: Crustal dilatation observed by GRACE after the 2004 Sumatra-Andaman earthquake, *Science, 313, 658-666,* doi:10.1126/science.1128661.

Heiskanen and Moritz 1967, Physical Geodesy

Heki K., and K. Matsuo, 2010: Coseismic gravity changes of the 2010 earthquake in Central Chile from satellite gravimetry, *Geophys. Res. Lett., 37,* L24306, doi:10.1029/2010GL045335.

Imanishi, Y., T. Sato, T. Higashi, W. Sun, and S. Okubo, 2004: A network of superconducting gravimeters detects submicrogal coseismic gravity changes, *Science, 306, 476-478.*

Kaula 1966, Theory of satellite geodesy: Applications of satellites to geodesy

Matsuo, K., and K. Heki, 2011: Coseismic gravity changes of the 2011 Tohoku-Oki Earthquake from satellite gravimetry, *Geophys. Res. Lett., 38,* L00G12, doi:10.1029/2011GL049018, 2011.

Ogawa, R., and K. Heki 2007: Slow postseismic recovery of geoid depression formed by the 2004 Sumatra - Andaman earthquake by mantle water diffusion, *Geophys. Res. Lett., 34*, L06313, doi:10.1029/2007GL029340.

Ozawa, S., T. Nishimura, H. Suito, T. Kobayashi, M. Tobita, and T. Imakiire, 2011: Coseismic and postseismic slip of the 2011 magnitude-9 Tohoku-Oki earthquake, *Nature,* doi:10.1038/nature10227.

Panet, I. et al., 2007. Coseismic and post-seismic signatures of the Sumatra 2004 December and 2005 March earthquakes in GRACE satellite gravity, *Geophys. J. Int., 171*, 177–190.

Rodell, M., and Houser, P. R., Jambor, U., Gottschalck, J., Mitchell, K., Meng, C.J., Arsenault, K., Cosgrove, B., Radakovich, J., Bosilovich, M., Entin, J.K., Walker, J.P., Lohmann, D., Toll, D., 2004: The Global Land Data Assimilation System. *Bull. Am. Meteorol. Soc. 85, 381-394.*

Sun, W., S. Okubo, G. Fu, and A. Araya, 2009: General formulations of global and co-seismic deformations caused by an arbitrary dislocation in a spherically symmetric earth model — applicable to deformed earth surface and space-fixed point, *Geophys. J. Int., 177, 817-833.*

Swenson, S., and J. Wahr, 2006: Post-processing removal of correlated errors in GRACE data, *Geophys. Res. Lett., 33,* L08402, doi:10.1029/2005GL025285.

Tanaka, Y., Okuno, J. and Okubo, S. (2006), A new method for the computation of global viscoelastic post-seismic deformation in a realistic earth model (I)—vertical displacement and gravity variation. *Geophys. J. Int.*, 164: 273–289. doi: 10.1111/j.1365-246X.2005.02821.x

Tanaka, Y., Okuno, J. and Okubo, S. 2007: A new method for the computation of global viscoelastic post-seismic deformation in a realistic earth model (II)-horizontal displacement. *Geophys. J. Int., 170: 1031–1052.* doi: 10.1111/j.1365-246X.2007.03486.x

Wahr, J., M. Molenaar, and F. Bryan, 1998: Time variability of the Earth's gravity field: Hydrological and oceanic effects and their possible detection using GRACE, J. Geophys. Res., 103, 30205-30229, doi:10.1029/98JB02844.

Wang, L., C.K. Shum, F. J. Simons, B. Tapley, and C. Dai 2012: Coseismic and postseismic deformation of the 2011 Tohoku-Oki eaerthquake constrained by GRACE gravimetry, *Geophys. Res. Lett., 39*, L07301, doi:10.1029/2012GL051104.

Zhang, Z., B. F. Chao, Y. Lu, and H. T. Hsu, 2009: An effective filtering for GRACE time-variable gravity: Fan filter, Geophys. Res. Lett., 36, L17311, doi: 10.1029/2009GL039459